Journal of Medicinal Chemistry

pubs.acs.org/jmc

Article

Constraining the Side Chain of C-Terminal Amino Acids in Apelin-13 Greatly Increases Affinity, Modulates Signaling, and Improves the Pharmacokinetic Profile

Kien Trân, Robin Van Den Hauwe, Xavier Sainsily, Pierre Couvineau, Jérôme Côté, Louise Simard, Marco Echevarria, Alexandre Murza, Alexandra Serre, Léa Théroux, Sabrina Saibi, Lounès Haroune, Jean-Michel Longpré, Olivier Lesur, Mannix Auger-Messier, Claude Spino, Michel Bouvier, Philippe Sarret,* Steven Ballet, and Éric Marsault

Cite This: *J. Med. Chem.* 2021, 64, 5345−5364

Read Online

ACCESS | Metrics & More | Article Recommendations | Supporting Information

ABSTRACT: Side-chain-constrained amino acids are useful tools to modulate the biological properties of peptides. In this study, we applied side-chain constraints to apelin-13 (Ape13) by substituting the Pro12 and Phe13 positions, affecting the binding affinity and signaling profile on the apelin receptor (APJ). The residues 1Nal, Trp, and Aia were found to be beneficial substitutions for Pro12, and the resulting analogues displayed high affinity for APJ (K_i 0.08−0.18 nM vs Ape13 K_i 0.7 nM). Besides, constrained (D-Tic) or α,α-disubstituted residues (Db_zg; D-α-Me-Tyr(OBn)) were favorable for the Phe13 position. Compounds **47** (Pro12-Phe13 replaced by Aia-Phe, K_i 0.08 nM) and **53** (Pro12-Phe13 replaced by 1Nal−Db_zg, K_i 0.08 nM) are the most potent Ape13 analogues activating the Gα_{12} pathways (**53**, EC_{50} Gα_{12} 2.8 nM vs Ape13, EC_{50} 43 nM) known to date, displaying high affinity, resistance to ACE2 cleavage as well as improved pharmacokinetics *in vitro* ($t_{1/2}$ 5.8−7.3 h in rat plasma) and *in vivo*.

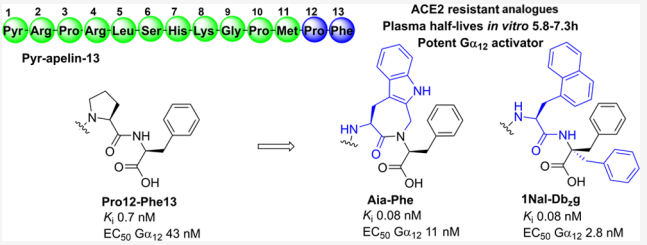

INTRODUCTION

Both apelin and the apelin receptor (APJ), a G-protein-coupled receptor (GPCR), have gained significant interest due to their involvement in a wide array of physiological processes like body fluid homeostasis, hypothalamic−pituitary−adrenal (HPA) axis regulation, and carbohydrate and lipid metabolism.[1−5] To date, potential applications of the apelinergic system have been largely centered on cardiovascular actions. As a strong inodilator, apelin exerts potent hypotensive action and positive inotropic effects, which concertedly reduce peripheral vascular resistance and increase cardiac output.[6−11] Apelin and its receptor are widely distributed in the vasculature and peripheral organs, including kidneys, lung, and heart.[11−15] Immunocytochemical localization revealed the presence of a high expression of APJ on human cardiomyocytes, vascular smooth muscle cells, and endothelial cells.[16] In the central nervous system, it is mainly expressed in the hypothalamic supraoptic and paraventricular nuclei, critical for body fluid homeostasis.[17,18] Even though much research has been dedicated to the apelinergic system, to date no apelin (receptor)-based pharmaceuticals are on the market, despite having been covered in multiple patents to date.[19] The majority of patents report the discovery of small-molecule agonists, yet clinical validation remains sparse and continued research is needed.[19]

Human apelin peptides include Pyr-apelin-13, apelin-17, and apelin-36, all derived from the proteolytic cleavage of a 77-mer prepropeptide, with Pyr-apelin-13 (Ape13) being predominant in both heart and plasma.[20,21] The downstream signaling cascades triggered upon APJ activation are highly complex, and their physiological impacts are not fully understood.[11] The apelin receptor mediates its physiological responses through the $G\alpha_{i/o}$ (in particular $G\alpha_{i1}$ and $G\alpha_{i2}$) and $G\alpha_{12/13}$ proteins.[11,22] The $G\alpha_i$-dependent pathway primarily inhibits cyclic adenosine monophosphate (cAMP) production and activates the extracellular-signal-regulated kinase (ERK) signaling cascade.[4,23] Several studies suggest that the $G\alpha_i$ pathway and ERK phosphorylation could correlate with some bioactivities of the apelinergic ligand, such as adipogenesis suppression,[24] body fluid homeostasis,[25] or protective effects in brain ischemia/reperfusion injury;[26] however, a direct link between those effects and $G\alpha_i$ activation still needs to be demonstrated. The $G\alpha_{12/13}$ pathway was also reported to be

Received: November 9, 2020
Published: February 1, 2021

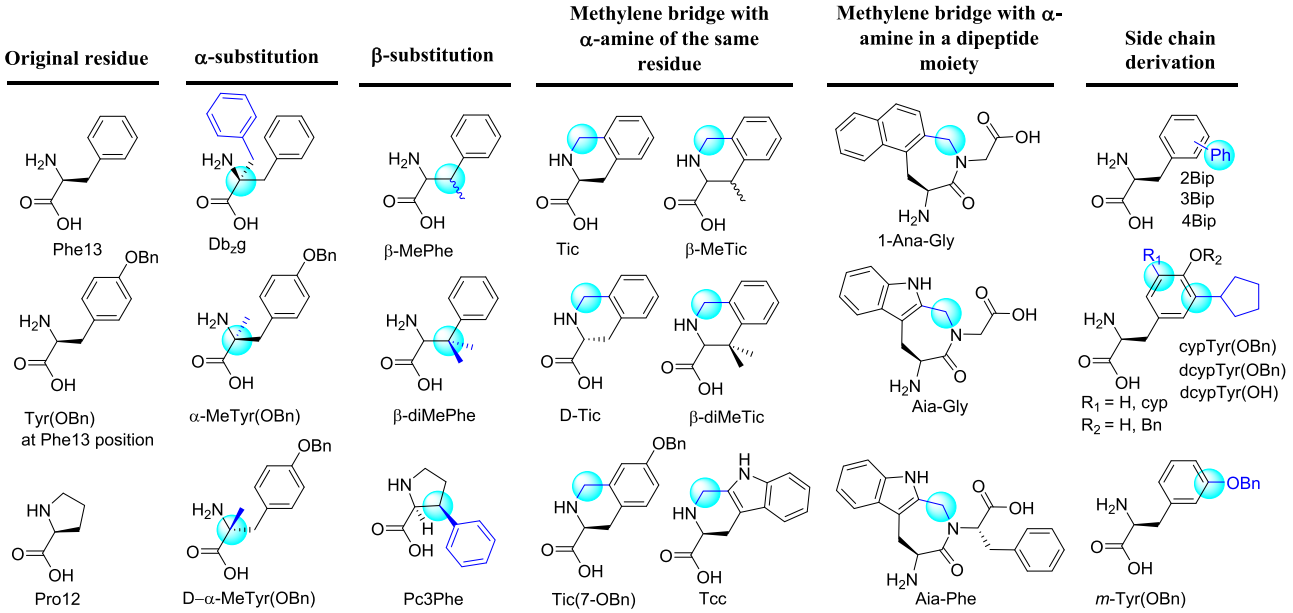

Figure 1. Conformationally constrained amino acids used in this study. Most unnatural amino acids were synthesized according to known procedures. Tic and D-Tic were purchased from commercial sources.

activated by apelin, leading to the activation of the MEF2 transcription factor and playing an important role in cardiovascular development in mice.[22] Besides, recent discovery showed that its signaling is influenced by the formation of APJ homodimer-oligomers or even heterodimer complexes with other GPCRs, such as kappa opioid (KOR), neurotensin type 1 (NTS1), angiotensin II type 1 (AT1), or bradykinin B2 (B2R) receptors.[27−31]

Upon activation, APJ is rapidly phosphorylated by GPCR kinases (GRK2 and GRK5), thereby increasing its affinity for β-arrestins.[32] Chronic activation may lead to receptor internalization due to the β-arrestin-mediated process, eventually resulting in desensitization and loss of therapeutic efficacy.[32] However, β-arrestin1/2 activation also plays an important role in GPCR signaling, acting as a "multifunctional scaffold" to recruit other intracellular signaling cascades.[33] For APJ, β-arrestin1/2 recruitment likely leads to the activation of the eNOS/NO pathway[7,34,35] and correlates with the hypotensive action of apelin[36,37] since ligands biased in disfavor of β-arrestin recruitment abolish both eNOS activation and vasodilation effect.[34,37,38] Other downstream signaling partners have been reported, such as PI3K/Akt, FoxO1/3, AMPK,[11,39] and the BK_{Ca} potassium channel,[40] although their coupling mechanisms and functions relative to APJ remain to be elucidated.

Interestingly, rapid internalization is promoted via interactions of the receptor with the C-terminal phenylalanine residue of apelin-13 analogues.[41] Indeed, deletion of Phe13 biases the receptor in favor of the $G\alpha_i$ over the β-arrestin pathway.[37] The corresponding Pyr-apelin-13[1−12] sequence retains most of the native peptide biological activity, yet structure−activity relationship (SAR) studies reveal that the introduction of unnatural amino acids at the C-terminus of the apelin peptide can significantly improve affinity and signaling potency.[42]

Apelin and Elabela, the other endogenous ligands of the apelin receptor, are prone to fast proteolytic degradation with half-lives under 5 min *in vivo*.[43−45] Several proteases have been identified to cleave apelin. These include the angiotensin-converting enzyme 2 (ACE2),[44,46] prolyl carboxypeptidase (PRCP),[47] neprilysin,[48] and human plasma kallikrein (KLKB1).[49] Excellent reviews discussing the biological implications of apelin analogues and their cognate receptor are available.[11,19,50−56] Of relevance to the current work, C-terminal modifications (Pro12 and Phe13) in apelin have been shown to drastically impact binding affinity and protease stability in both plasma and cerebrospinal fluid.[43,57] The Phe13 C-terminus is the master switch for binding affinity and receptor activation.[37,38,42] Its mutation into Ala reduces the binding affinity, and the resulting compound (F13A) could antagonize the Ape13 effect on blood pressure.[38] Moreover, previous work by our group has shown that replacing Phe13 with *p*-benzoyl-L-phenylalanine (Bpa) or α-MePhe provides potent analogues with affinities in the sub-nM range and 30-fold improvement in cAMP production inhibition. Additionally, replacement of Phe13 with Tyr(OBn) resulted in the highest affinity APJ ligands reported to date (K_i 0.02 nM).[42] For the Pro12 position, D-scan and Ala-scan showed that it does not play an important role in ligand binding.[58,59] However, substitution in this position by proline mimetics (Aib, Acpc) may affect peptide stability since several enzymes (ACE2, PRCP) cleave the amide bond between Pro12 and Phe13.[44,58,59] Altogether, the C-terminal extremity of Ape13 emerges as a critical determinant of affinity, signaling, and stability. To fine-tune these properties and provide compounds with further improved properties, we describe herein the synthesis of modified Ape13 peptides in which the Pro12 and Phe13 residues were substituted with a large set of unnatural, conformationally constrained amino acids and measured the impact of the modifications on the resulting pharmacological properties.

The affinity of modified analogues for APJ was determined by a competitive radioligand binding assay against [^{125}I][Nle^{75}, Tyr^{77}]Pyr-apelin-13. Their ability to trigger the activation of the $G\alpha_{i1}$, $G\alpha_{12}$, and β-arrestin2 pathways was assessed using bioluminescence resonance energy transfer

https://dx.doi.org/10.1021/acs.jmedchem.0c01941
J. Med. Chem. 2021, 64, 5345−5364

(BRET)-based biosensors using HEK293 cells.[60] The proteolytic stability of selected compounds was evaluated separately against rat plasma and recombinant rat ACE2 enzyme. Finally, potent analogues were chosen for further pharmacokinetic studies and an assessment on blood pressure *in vivo*.

RESULTS AND DISCUSSION

Synthesis. Unnatural amino acids were selected as close analogues of Phe or Pro possessing side chains constrained in different ways (Figure 1). This includes the introduction of substituents at the α- or β-position (e.g., α,α-dibenzylglycine (Db$_z$g), α-MeTyr(OBn), β-MePhe), formation of a methylene bridge with the α-amine of the peptide backbone (e.g., Tic, Ana, or Aia derivatives), or side-chain derivatization (e.g., Bip, cypTyr(OBn)), all synthesized according to known procedures.[61−64] The description of their syntheses can be found in the Electronic Supporting Information section of this manuscript (ESI, Sections 2−4). Additionally, several unnatural amino acids are reported for the first time in this manuscript, such as β-diMeTic (**6**), cypTyr(OBn) (**15a**), and dcypTyr(OBn) (**15b**). Their syntheses are described in the Experimental Section. Moreover, a new asymmetric synthesis for D-α-MeTyr(OBn) (**22**) is also presented.

Constrained amino acids **5** and **6** were prepared starting from a modified literature procedure (Scheme 1).[62] First,

Scheme 1. Synthesis of Fmoc-β-dimethyl-Phe/Tic-OH (5/6)[a]

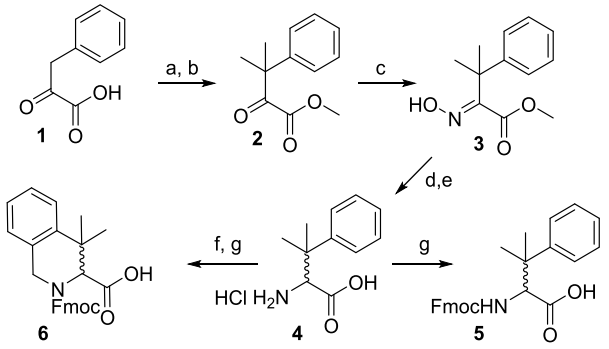

[a](a) MeI, NaOH, THF rt, 89%; (b) $SOCl_2$, MeOH reflux, 90%; (c) $NH_2OH.HCl$, MeOH, 65 °C, 94%; (d) Zn, 30% H_2SO_4, AcOH, reflux, 66%; (e) 1 N HCl/acetone, reflux, 99%; (f) 12 N HCl, formalin, reflux, 72%; (g) Fmoc-OSu, Na_2CO_3, acetone/water, rt, 76% for **5** and 71% for **6**.

methylation at the β-position of commercial phenylpyruvic acid **1** was performed using MeI and NaOH in tetrahydrofuran (THF). Subsequent esterification was achieved with thionyl-chloride in methanol, followed by oxime synthesis using hydroxylamine as a nucleophile in dry MeOH. Reduction of oxime **3** with zinc powder provided the corresponding amino ester, which was saponified in standard conditions to deliver the pivotal amino acid intermediate **4** as a racemate. The latter was Fmoc-protected to give Fmoc-βdiMe-Phe-OH **5** or underwent a Pictet−Spengler reaction to cleanly deliver the corresponding six-membered isoquinoline. Crystallization of this intermediate was achieved upon cooling, and final Fmoc-protection provided Fmoc-βdiMe-Tic-OH **6**.

To further explore the impact of C-terminal modifications, two azepinone-based constraints were implemented (**11a**, **11b**, Scheme 2). Linkage of the aromatic side chain to the amine of the next amino acid in the sequence not only allows χ-space

Scheme 2. Synthesis of Fmoc-Aia-Gly-OH 11a and Fmoc-Aia-Phe 11b[a]

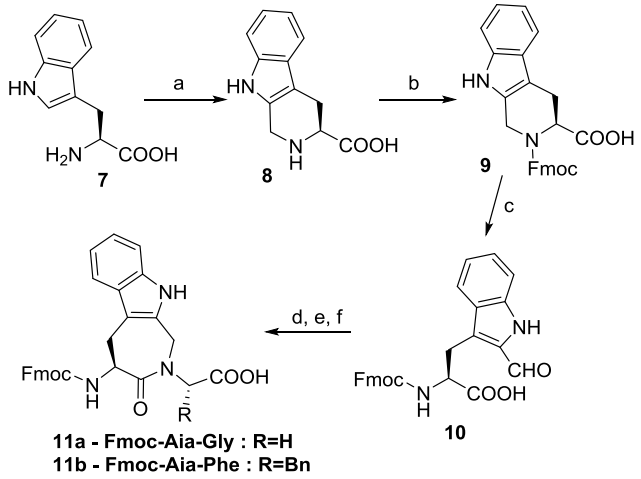

[a](a) cat. H_2SO_4 formalin, rt, 4 h, 49%; (b) Fmoc-OSu, Na_2CO_3, acetone/H_2O, rt, 16 h, 71%; (c) SeO_2, dioxane, reflux, 2 h, 45%; (d) $NaCNBH_3$, CH_2Cl_2, HCl.H_2N-Gly-OMe or HCl.H_2N-Phe-OMe, NMM, AcOH, rt; (e) EDC HCl, ACN/H_2O, pyridine, rt, 48 h; (f) 1 N HCl/acetone, 90 °C, 16 h. **11a**: 40% (three steps for **11a**), **11b:** 21% (three steps for **11b**).

screening, it is also a great tool to increase metabolic stability of the corresponding analogues.[63] Hence, we synthesized three different azepinones-containing dipeptides Aia-Gly, Aia-Phe, and 1-Ana-Gly (Figure 1) following known procedures.[64] Synthesis of the indoloazepinone-constrained Aia started by ring-closing L-Trp using the Pictet−Spengler reaction, followed by Fmoc-protection of the amine to deliver **9**. Formation of the corresponding aldehyde **10** enabled incorporation of a second amino acid via reductive amination. After formation of the secondary amine, ring closure using EDC·HCl by intramolecular coupling yielded the indoloazepinone scaffold. Dipeptides **11a** and **11b** were obtained after final ester hydrolysis. The synthesis of Fmoc-1-Ana-Gly-OH (not shown) was completely performed as described previously.[65]

In past works, Tyr(OBn) substitution of Phe13 on Ape13 was shown to increase affinity down to the pM level.[42] For this reason, the Tyr(OBn) residue was used as a scaffold to implement conformational constraints. Constrained analogues Tic(7-OBn) and *m*-Tyr(OBn) were easily prepared from commercially available starting materials (Figure 1; see the Supporting Information for syntheses). On the other hand, analogues cypTyr(OBn) and dcypTyr(OBn) were synthesized from unprotected L-tyrosine (Scheme 3A). First, 3′-C-alkylation of L-Tyr **12** was performed with cyclopentanol in H_3PO_4 85% at 100 °C.[66] This reaction yielded a mixture of mono- and dialkylated products, cypTyr **13a** and dcypTyr **13b**, which were separated after subsequent *N*-Alloc protection. *O*-alkylation and hydrolysis were then carried out to deliver *N*-Alloc-cypTyr(OBn) **15a** and *N*-Alloc-dcypTyr(OBn) **15b**, used as building blocks in solid-phase synthesis. Peptidic analogues containing dcypTyr(OH) were generated from those having dcypTyr(OBn) by increasing the peptide cleavage time up to 4 h with a mixture of trifluoroacetic acid (TFA)/triisopropylsilane (TIPS)/H_2O (95:2.5:2.5).

https://dx.doi.org/10.1021/acs.jmedchem.0c01941
J. Med. Chem. 2021, 64, 5345−5364

Scheme 3. Synthetic Scheme of Tyr(OBn) Analogues[a]

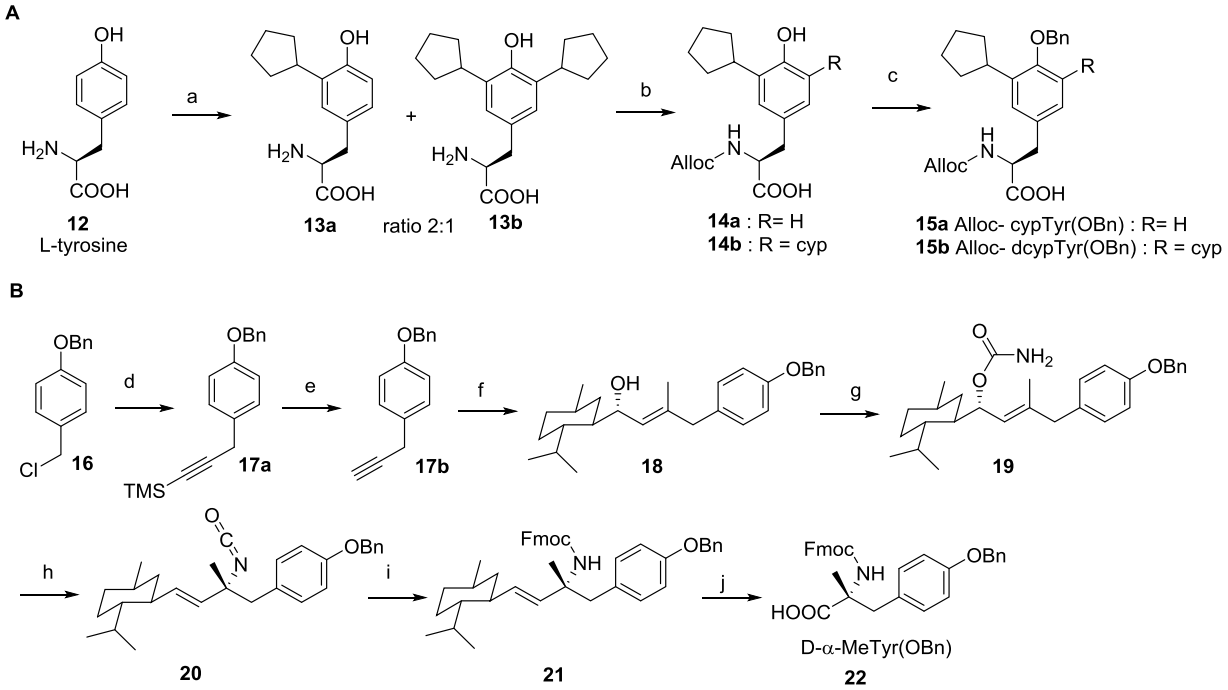

[a](A) (a) cyclopentanol, H_3PO_4 85%, 100 °C, 16 h; (b) allyl chloroformate (1.2 equiv), $NaHCO_3$, THF-H_2O (1:1), rt, 15 min, 55%; (c) (i) BnBr, K_2CO_3, acetonitrile reflux, 1 h, 73−77%; (ii) KOH 2 M, 1.2 equiv, EtOH-H_2O (5:1), 70 °C, 15 min, 83−85%; (B) (d) tetramethylsilane (TMS)−acetylene, CuI, K_2CO_3, tetrabutylammonium iodide (TBAI), acetonitrile, 40 °C, 24 h, 94%; (e) MeOH, K_2CO_3, rt, 1.5 h, 88%; (f) (i), $AlMe_3$, $ZrCp_2Cl_2$, dichloromethane (DCM), rt, 16 h; (ii), *p*-menthyl-3-carboxaldehyde, THF, −78 °C, 2 h, 47%; (g) (i), trichloroacetyl isocyanate, DCM, 0 °C, 1 h; (ii), MeOH, K_2CO_3, rt, 16 h, 72%; (h) TFAA, TEA, DCM, 0 °C, 15 min, 95%; (i) $Ti(OtBu)_4$, 9-fluorenemethanol, benzene, 45 °C, 3 h, 75%; (j) (i), ozone, PPh_3, DCM, rt, 15 h; (ii), NaOCl, *tert*-butanol-H_2O (1:1), rt, 16 h, 67%.

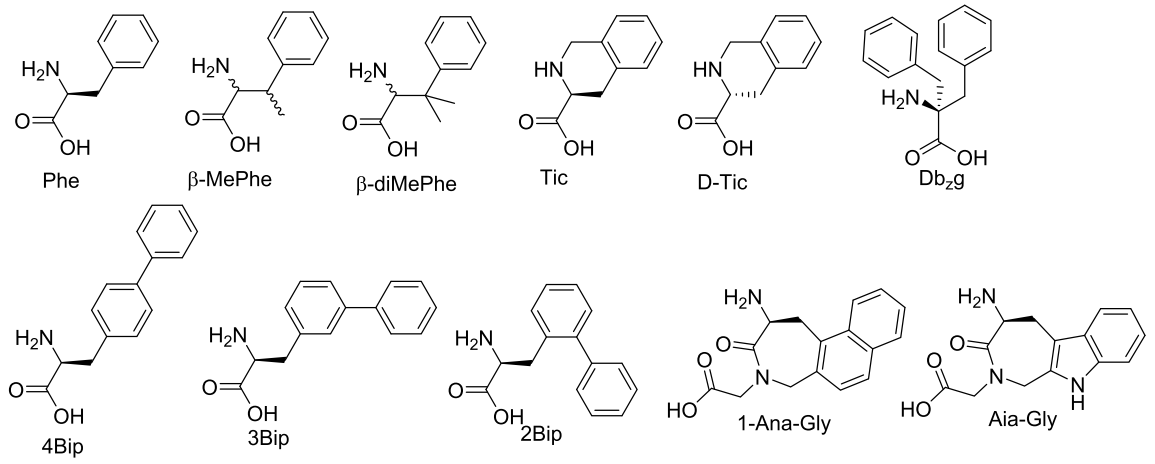

Figure 2. Unnatural amino acids used to modify Phe13 of Pyr-apelin-13.

The L-α-MeTyr(OBn) residue was prepared from commercially available L-α-MeTyr, whereas the D-α-MeTyr(OBn) analogue was synthesized from 4-(benzyloxy)benzyl chloride **16** using *p*-menthyl-3-carboxaldehyde as a chiral auxiliary (Scheme 3B).[67] Critical steps in this synthesis are the Zr-catalyzed carboalumination of the triple bond of intermediate **17b**, followed by trapping of the vinylalane intermediate with *p*-menthyl-3-carboxaldehyde to produce chiral allylic alcohol **18** as a single detected diastereomer. The α-nitrogen was introduced using trichloroacetyl isocyanate, first forming carbamate **19**, followed by [3,3]-sigmatropic rearrangement to construct the asymmetric center of the α-amino acid precursor in the form of isocyanate **20**. The latter was converted to Fmoc-protected amine **21** by reaction with 9-fluorenemethanol. Finally, the chiral auxiliary was cleaved to give the desired Fmoc-D-α-MeTyr(OBn) **22** ready for incorporation in Ape13.

Impact of Modifications on Binding Affinity and Functional Activities. *Impact of Modifications of Phe13.* Phe13 is an important residue for activation of the downstream signaling pathway of the apelin receptor.[37] As receptor binding is a dynamic process, the side chain of Phe13 may adopt several conformations as suggested by molecular dynamics simulations.[41,68] For this reason, we decided to constrain its side chain in different ways (Figure 2 and Table 1) to explore

https://dx.doi.org/10.1021/acs.jmedchem.0c01941
J. Med. Chem. 2021, 64, 5345−5364

Table 1. Affinity and Functional Activities of Phe13-Modified Pyr-apelin-13 Analogues

	peptide sequence	binding K_i (nM)[a]	$G\alpha_{i1}$ EC_{50} (nM)[b]	$G\alpha_{12}$ EC_{50} (nM)[c]	β-arr2 EC_{50} (nM)[d]
Ape13	Pyr-R-P-R-L-S-H-K-G-P-M-P-F	0.7 ± 0.1	1.1 ± 0.1	43 ± 1	40 ± 4
23	Pyr-R-P-R-L-S-H-K-G-P-Nle-P-(**β-MePhe**)-**OH**	0.37 ± 0.04	1.0 ± 0.2	108 ± 6	40 ± 7
24	Pyr-R-P-R-L-S-H-K-G-P-Nle-P-(**β-diMePhe**)-**OH**	0.36 ± 0.01	2.4 ± 0.3	67 ± 3	69 ± 7
25	Pyr-R-P-R-L-S-H-K-G-P-Nle-P-**Tic-OH**	1.1 ± 0.1	2.5 ± 0.7	88 ± 4	67 ± 10
26	Pyr-R-P-R-L-S-H-K-G-P-Nle-P-(**d-Tic**)-**OH**	0.07 ± 0.03	1.0 ± 0.1	23 ± 3	10 ± 2
27	Pyr-R-P-R-L-S-H-K-G-P-Nle-P-**Db$_z$g-OH**	0.04 ± 0.01	1.5 ± 0.4	10 ± 2	19 ± 2
28	Pyr-R-P-R-L-S-H-K-G-P-Nle-P-(**4-Bip**)-**OH**	0.35 ± 0.01	2.1 ± 0.4	21 ± 1	64 ± 4
29	Pyr-R-P-R-L-S-H-K-G-P-Nle-P-(**3-Bip**)-**OH**	0.31 ± 0.01	1.4 ± 0.4	24 ± 1	47 ± 4
30	Pyr-R-P-R-L-S-H-K-G-P-Nle-P-(**2-Bip**)-**OH**	2.8 ± 0.1	8.6 ± 2.8	142 ± 4	391 ± 11
31	Pyr-R-P-R-L-S-H-K-G-P-Nle-P-(**1-Ana-Gly**)-**OH**	1.7 ± 0.5	6.4 ± 1.1	74 ± 4	221 ± 34
32	Pyr-R-P-R-L-S-H-K-G-P-Nle-P-**Aia-Gly-OH**	4.3 ± 0.3	6.8 ± 1.6	481 ± 12	311 ± 82

[a] K_i was calculated from experimental IC_{50} values (the concentration of ligand that displaces 50% of radiolabeled [^{125}I][Nle^{75}, Tyr^{77}]Pyr-apelin-13) using the Cheng−Prusoff equation.[69] Values represent the mean ± standard error of the mean (SEM) of two to three experiments, each performed in duplicate. [b] EC_{50} corresponds to the concentration of ligand that produces 50% dissociation of $G\alpha_{i1}$ from the $G\beta\gamma$ subunits. [c] EC_{50} corresponds to the concentration of ligand that produces 50% recruitment of the $G\alpha_{12}$ effector (PDZ-RhoGEF) to the cell membrane. [d] EC_{50} is the concentration of ligand that produces 50% recruitment of β-arrestin2 to the apelin receptor. Values represent the mean ± SEM of three experiments, each performed in triplicate.

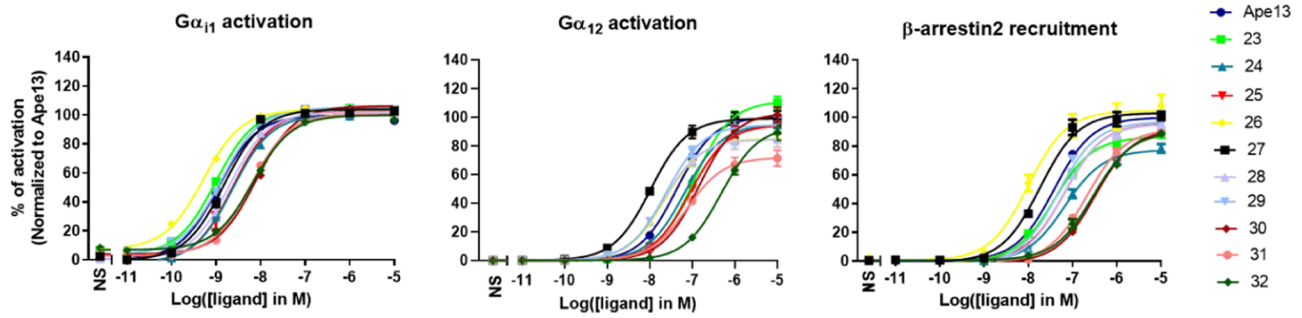

Figure 3. BRET dose−response curves of $G\alpha_{i1}$, $G\alpha_{12}$, and β-arrestin2 pathways of Ape13 analogues with modification of Phe13.

how the modulation of this side chain impacts the binding affinity and signaling profile.

First, methyl substitutions were introduced at the β-position of Phe13 to restrict rotations of its side chain in the χ space.[65] Mono- or dimethyl substitutions on racemic Phe showed little effect on ligand binding profiles (**23**, K_i 0.37 nM; **24**, K_i 0.36 nM vs Ape13, K_i 0.7 nM), and no significant impact on signaling was observed. Despite a slight increase in affinity of this epimeric mixture (<2-fold), the possibility that one epimer may provide better affinity than the other cannot be ruled out. In contrast, cyclic constraint of the aromatic side chain into Tic analogues produced interesting effects. L-Tic substitution resulted in a slight decrease in binding affinity (**25**, K_i 1.1 nM), while D-Tic led to a 10-fold increase in binding (**26**, K_i 0.07 nM vs Ape13, K_i 0.7 nM). Our previous study showed that chiral inversion of Phe13 to D-Phe on Ape13 results in a loss of binding affinity to the apelin receptor,[58] which is quite different compared to this result. It is plausible that the structural constraint of D-Tic may keep the side chain in a favorable conformation for receptor binding, which is less accessible by free rotation in the D-Phe side chain or, alternatively, impacts the peptide backbone's conformation. Substitution at the α-position also brings benefits, as observed with the α,α-dibenzylglycine analogue, which displays a 17-fold increase in binding affinity (**27**, K_i 0.04 nM).

To probe the space around the aromatic ring of Phe13, we also introduced a phenyl substituent at the ortho-, meta-, and para-positions of this residue. Analogues containing 3-Bip and 4-Bip demonstrate similar activities compared to the endogenous ligand (**28**, K_i 0.35 nM; **29**, K_i 0.31 nM), while 2-Bip substitution slightly reduces the binding affinity (**30**, K_i 2.8 nM vs Ape13, K_i 0.7 nM). Altogether, these results suggest that there is significant room to accommodate aromatic residues around the Phe aryl group. This is congruent with previous results consisting of replacing Phe13 by 1-Nal, 2-Nal, or Tyr(OBn).[58]

Side-chain-constrained dipeptide analogues, such as 1-Ana-Gly (**31**) or Aia-Gly (**32**), were also introduced at the Phe13 position. They both allow the carboxylate group to extend deeper into the binding pocket since an additional glycine is inserted. Although the affinity of these analogues does not increase, it stays in the low nM level (**31**, K_i 1.7 nM; **32**, K_i 4.3 nM vs Ape13, K_i 0.7 nM), underlining that the binding pocket has a considerable degree of flexibility and is able to accommodate additional residues at the C-terminus of Ape13.

Regarding signaling, compounds showing good binding affinity, such as **26** (K_i 0.07 nM) and **27** (K_i 0.04 nM), also display excellent potency in activating signaling pathways (Figure 3). Indeed, compound **27** is around fourfold superior at $G\alpha_{12}$ activation (EC_{50} $G\alpha_{12}$ 10 nM) compared to the endogenous ligand (Ape13, EC_{50} $G\alpha_{12}$ 43 nM). Moreover, analogues **26** (Phe13 → D-Tic) and **27** (Phe13 → Db$_z$g) exhibit EC_{50} on β-arrestin2 recruitment at 10 and 19 nM, respectively, which is two- to fourfold better than that of Ape13 (EC_{50} β-arr2 40 nM) and makes them some of the most potent activators of the β-arrestin2 pathway. Despite such improvements in binding and $G\alpha_{12}$ and β-arrestin pathways, the potency of $G\alpha_{i1}$ activation of **26** and **27** stays at the same

https://dx.doi.org/10.1021/acs.jmedchem.0c01941
J. Med. Chem. 2021, 64, 5345−5364

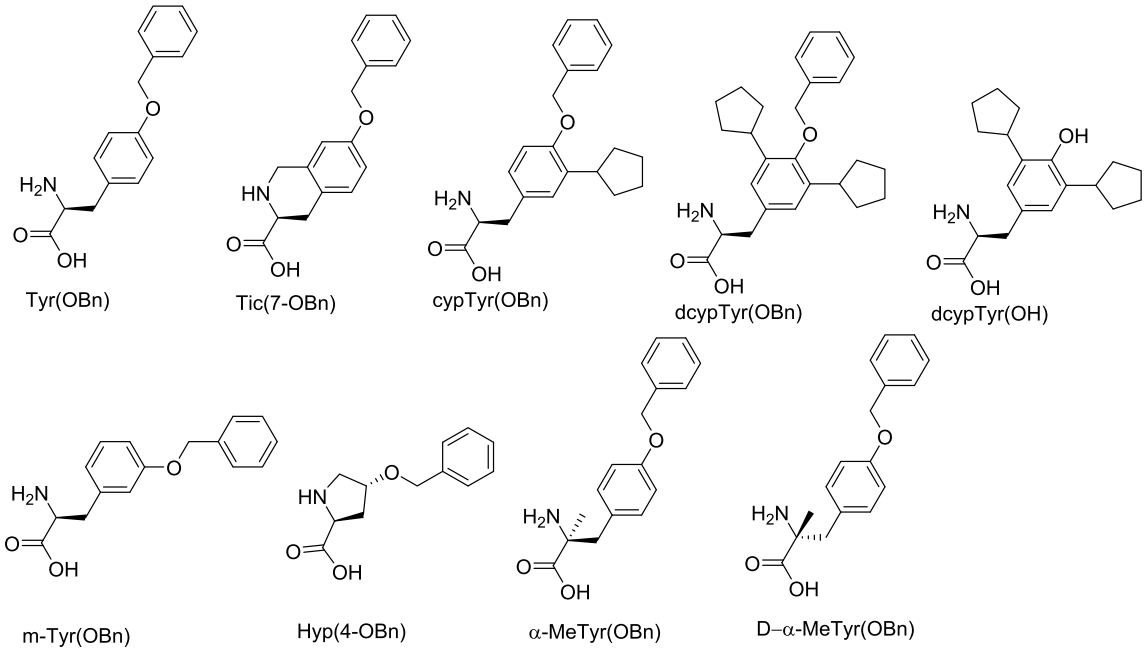

Figure 4. Unnatural analogues of Tyr(OBn) used to replace Phe13.

Table 2. Affinity and Functional Activities of Pyr-apelin-13 Analogues Containing Tyr(OBn) Surrogates

	peptide sequence	binding K_i (nM)[a]	$G\alpha_{i1}$ EC_{50} (nM)[b]	$G\alpha_{12}$ EC_{50} (nM)[c]	β-arr2 EC_{50} (nM)[d]
Ape13	Pyr-R-P-R-L-S-H-K-G-P-M-P-F	0.7 ± 0.1	1.1 ± 0.1	43 ± 1	40 ± 4
33	Pyr-R-P-R-L-S-H-K-G-P-Nle-P-**Tyr(OBn)-OH**	0.02 ± 0.003	0.5 ± 0.2	11 ± 6	14 ± 6
34	Pyr-R-P-R-L-S-H-K-G-P-Nle-P-**Tic(7-OBn)-OH**	0.19 ± 0.06	3.4 ± 1.0	22 ± 6	45 ± 6
35	Pyr-R-P-R-L-S-H-K-G-P-Nle-P-**cypTyr(OBn)-OH**	0.41 ± 0.13	5.7 ± 3.1	53 ± 9	69 ± 14
36	Pyr-R-P-R-L-S-H-K-G-P-Nle-P-**dcypTyr(OBn)-OH**	13 ± 0.4	22 ± 8	141 ± 30	367 ± 128[e]
37	Pyr-R-P-R-L-S-H-K-G-P-Nle-P-**dcypTyr(OH)-OH**	1.6 ± 0.2	16 ± 5	111 ± 30	361 ± 7
38	Pyr-R-P-R-L-S-H-K-G-P-Nle-P-(***m*-Tyr(OBn)**)-OH	0.46 ± 0.05	3.8 ± 0.4	45 ± 9	106 ± 12
39	Pyr-R-P-R-L-S-H-K-G-P-Nle-P-**Hyp(4-OBn)-OH**	6.1 ± 0.3	6.4 ± 1.8	63 ± 27	192 ± 61
40	Pyr-R-P-R-L-S-H-K-G-P-Nle-P-(**l-α-MeTyr(OBn)**)-OH	1.0 ± 0.2	19 ± 9	11 ± 1	571 ± 57
41	Pyr-R-P-R-L-S-H-K-G-P-Nle-P-(**d-α-MeTyr(OBn)**)-OH	0.12 ± 0.08	2.7 ± 0.9	4.4 ± 0.5[f]	30 ± 1

[a] K_i was calculated from experimental IC_{50} values (the concentration of ligand that displaces 50% of radiolabeled [^{125}I][Nle^{75}, Tyr^{77}]Pyr-apelin-13) using the Cheng–Prusoff equation.[69] Values represent the mean ± SEM of two to three experiments, each performed in duplicate. [b] EC_{50} corresponds to the concentration of ligand that produces 50% dissociation of $G\alpha_{i1}$ from the $G\beta\gamma$ subunits. [c] EC_{50} corresponds to the concentration of ligand that produces 50% recruitment of the $G\alpha_{12}$ effector (PDZ-RhoGEF) to the cell membrane. [d] EC_{50} is the concentration of ligand that produces 50% recruitment of β-arrestin2 to the apelin receptor. Values represent the mean ± SEM of three experiments, each performed in triplicate. Most compounds showed E_{max} > 75%, except for **36** in the β-arrestin2 pathway and **41** in the $G\alpha_{12}$ pathway. [e] E_{max} 53%. [f] E_{max} 46%.

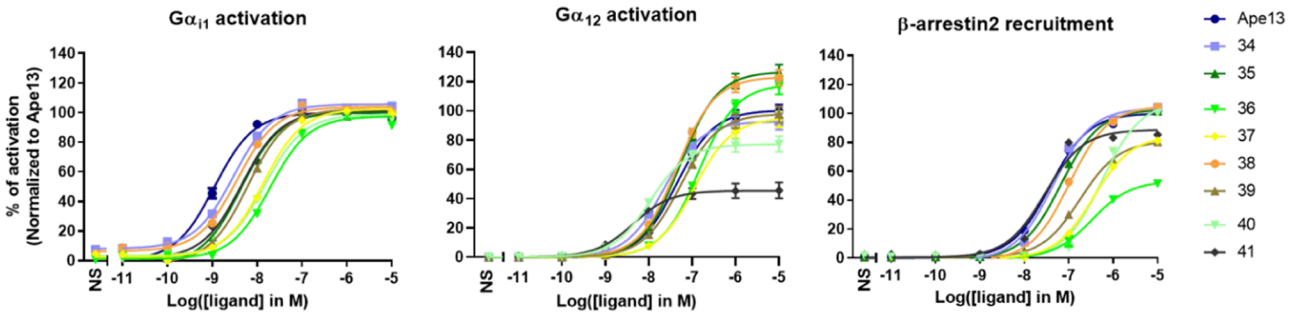

Figure 5. BRET dose–response curves of $G\alpha_{i1}$, $G\alpha_{12}$, and β-arrestin2 pathways of Ape13 analogues with Tyr(OBn) derivatives on the Phe13 position.

level as those of Ape13 (EC_{50} $G\alpha_{i1}$ 1–1.5 nM). In contrast, Aia-Gly (**32**, K_i 4.3 nM) or 2-Bip (**30**, K_i 2.8 nM) substitution displays 6- to 10-fold lower potency in all examined signaling pathways, which goes in the same direction as their affinity.

In conclusion, although the binding pocket of Phe13 displays a high tolerance for side-chain modifications and even Phe13 replacement by dipeptide moieties, it still shows preference for a certain type of constrained residues, such as

https://dx.doi.org/10.1021/acs.jmedchem.0c01941
J. Med. Chem. 2021, 64, 5345–5364

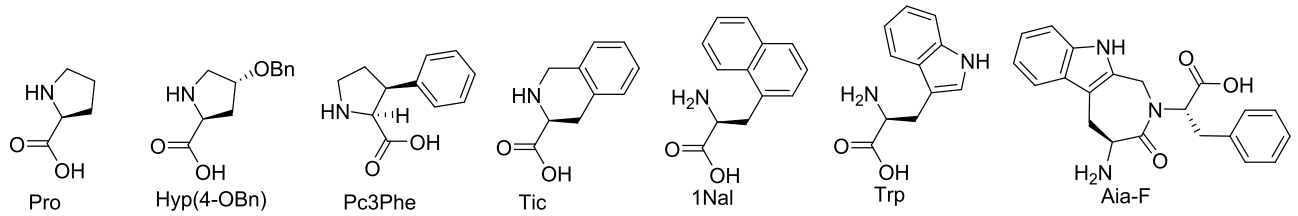

Figure 6. Unnatural amino acids used to modify Pro12 of Pyr-apelin-13.

Table 3. Affinity and Functional Activities of Pro12-Modified Pyr-apelin-13 Analogues

	peptide sequence	binding K_i (nM)[a]	$G\alpha_{i1}$ EC_{50} (nM)[b]	$G\alpha_{12}$ EC_{50} (nM)[c]	β-arr2 EC_{50} (nM)[d]
Ape13	Pyr-R-P-R-L-S-H-K-G-P-M-P-F	0.7 ± 0.1	1.1 ± 0.1	43 ± 1	40 ± 4
42	Pyr-R-P-R-L-S-H-K-G-P-Nle-**Hyp(4-OBn)**-F-OH	2.1 ± 0.3	5.6 ± 0.6	54 ± 1	100 ± 9
43	Pyr-R-P-R-L-S-H-K-G-P-Nle-**Pc3Phe**-F-OH	4.2 ± 0.7	17 ± 3	48 ± 2	454 ± 75
44	Pyr-R-P-R-L-S-H-K-G-P-Nle-**Tic**-F-OH	9.7 ± 0.8	9.6 ± 5.1	67 ± 2	142 ± 18
45	Pyr-R-P-R-L-S-H-K-G-P-Nle-**1Nal**-F-OH	0.12 ± 0.01	4.4 ± 0.6	9.2 ± 0.2	41 ± 4
46	Pyr-R-P-R-L-S-H-K-G-P-Nle-**Trp**-F-OH	0.18 ± 0.02	3.8 ± 0.6	17 ± 3	38 ± 2
47	Pyr-R-P-R-L-S-H-K-G-P-Nle-**Aia**-F-OH	0.08 ± 0.01	2.5 ± 0.3	11 ± 1	25 ± 5

[a] K_i was calculated from experimental IC_{50} values (the concentration of ligand that displaces 50% of radiolabeled [^{125}I][Nle^{75}, Tyr^{77}]Pyr-apelin-13) using the Cheng−Prusoff equation.[69] Values represent the mean ± SEM of two to three experiments, each performed in duplicate. [b] EC_{50} corresponds to the concentration of ligand that produces 50% dissociation of $G\alpha_{i1}$ from the $G\beta\gamma$ subunits. [c] EC_{50} corresponds to the concentration of ligand that produces 50% recruitment of the $G\alpha_{12}$ effector (PDZ-RhoGEF) to the cell membrane. [d] EC_{50} is the concentration of ligand that produces 50% recruitment of β-arrestin2 to the apelin receptor. Values represent the mean ± SEM of three experiments, each performed in triplicate.

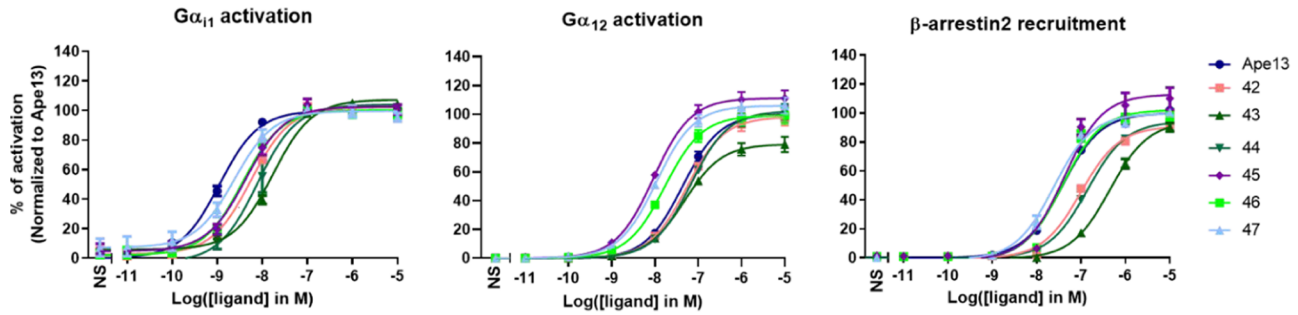

Figure 7. BRET dose−response curves of $G\alpha_{i1}$, $G\alpha_{12}$, and β-arrestin2 pathways of Ape13 analogues with modification on Pro12.

constrained D-amino acid (D-Tic) or the α,α-disubstituted analogue Db_zg.

Impact of Replacements of Phe13 by Tyr(OBn) Analogues. We reported previously that the Tyr(OBn) substitution is favorable at the Phe13 position of Ape13, providing a 60-fold increase in binding affinity (**33**, K_i 0.02 nM).[42] To explore more thoroughly the binding pocket around this key residue and find out whether close derivatives of Tyr(OBn) bring similar benefits, we developed several analogues where the side chain is either constrained, such as Tic(7-OBn) (**34**, K_i 0.19 nM), or bears sterically hindered groups in the ortho-position of the benzyloxy moiety, such as cypTyr(OBn) (**35**, K_i 0.41 nM), dcypTyr(OBn) (**36**, K_i 13 nM), or dcypTyr(OH) (**37**, K_i 1.6 nM) (Figure 4 and Table 2). These modifications were in general well-tolerated with the exception of dcypTyr-(OBn), which seems too bulky for the binding pocket. Similarly, substitution of Phe13 with *m*-Tyr(OBn) (**38**, K_i 0.46 nM) does not provide the same improvement as Tyr(OBn) (**33**, K_i 0.02 nM), while replacement by 4-benzyloxyproline Hyp(4-OBn) (**39**, K_i 6.1 nM) seems less tolerated. The affinity reduction of **39** compared to its analogue **33** could be explained by the fact that Hyp(4-OBn) substitution changes the benzyloxy group position, the backbone conformation, as well as the orientation of the carboxylate pharmacophore on the C-terminal tail.

The effect of substitution on the α-carbon of the C-terminal Tyr(OBn) analogue was also investigated. Introduction of a methyl group at this position, providing the L-α-MeTyr(OBn) analogue, did not produce sub-nM affinity ligands as expected (**40**, K_i 1.0 nM vs Tyr(OBn), **33**, K_i 0.02 nM). However, stereoinversion to D-α-MeTyr(OBn) leads to analogue **41** displaying an affinity constant at the sub-nM range (**41**, K_i 0.12 nM). Remarkably, the two epimers display a 10-fold difference in binding affinity.

Substitution of Phe13 with Tyr(OBn) analogues significantly alters the signaling profile of the resulting ligands. The α-substituted analogues **40** (K_i 1.0 nM) and **41** (K_i 0.12 nM) display excellent potencies at $G\alpha_{12}$ activation (EC_{50} $G\alpha_{12}$ 11 and 4.4 nM, respectively), equal to or slightly better than the reference analogue with Tyr(OBn) (**33**, EC_{50} $G\alpha_{12}$ 11 nM) and clearly superior to Ape13 (EC_{50} 43 nM). While analogue **40** provides good potency on $G\alpha_{12}$ pathways, it is much weaker on both the $G\alpha_{i1}$ and β-arrestin2 pathways, suggesting a biased profile in favor of $G\alpha_{12}$. Besides, the maximum efficacy of **41** on the $G\alpha_{12}$ pathway is significantly reduced, reaching only 46% of the maximum response (E_{max}) of Ape13, as

https://dx.doi.org/10.1021/acs.jmedchem.0c01941
J. Med. Chem. 2021, 64, 5345−5364

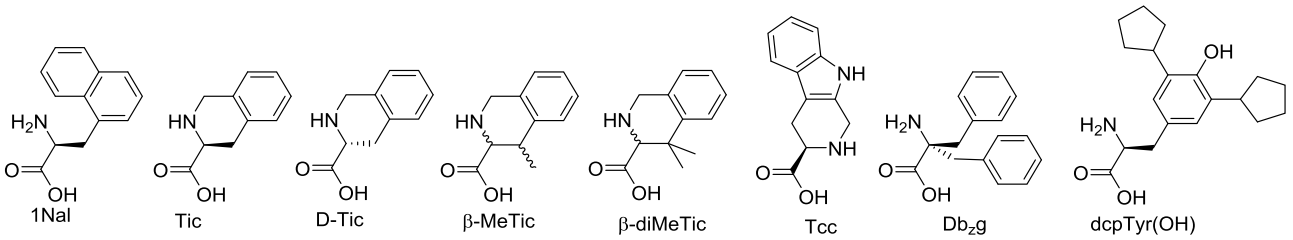

Figure 8. Unnatural amino acids used to modify Phe13 in combination with the substitution of 1-Nal on Pro12.

Table 4. Affinity and Functional Activities of Pyr-apelin-13 Analogues with Combined Modification of Pro12 and Phe13

	peptide sequence	binding K_i (nM)[a]	Gα_{i1} EC_{50} (nM)[b]	Gα_{12} EC_{50} (nM)[c]	β-arr2 EC_{50} (nM)[d]
Ape13	Pyr-R-P-R-L-S-H-K-G-P-M-P-F	0.7 ± 0.1	1.1 ± 0.1	43 ± 1	40 ± 4
33	Pyr-R-P-R-L-S-H-K-G-P-Nle-P-**Tyr(OBn)-OH**	0.02 ± 0.003	0.5 ± 0.2	11 ± 6	14 ± 6
45	Pyr-R-P-R-L-S-H-K-G-P-Nle-**1Nal**-F-OH	0.12 ± 0.01	4.4 ± 0.6	9.2 ± 0.2	41 ± 4
48a	Pyr-R-P-R-L-S-H-K-G-P-Nle-**1Nal**-Tic-OH	0.09 ± 0.01	1.6 ± 0.3	15 ± 2	32 ± 2
48b	Pyr-R-P-R-L-S-H-K-G-P-Nle-**2Nal**-Tic-OH	0.37 ± 0.01	4.3 ± 0.3	n/a[e]	94 ± 9
49	Pyr-R-P-R-L-S-H-K-G-P-Nle-**1Nal-(d-Tic)**-OH	0.08 ± 0.01	4.2 ± 0.9	28 ± 1	33 ± 4
50	Pyr-R-P-R-L-S-H-K-G-P-Nle-**1Nal-(β-MeTic)**-OH	0.40 ± 0.17	4.3 ± 0.5	111 ± 6	44 ± 4
51	Pyr-R-P-R-L-S-H-K-G-P-Nle-**1Nal-(β-diMeTic)**-OH	0.16 ± 0.04	4.1 ± 0.9	10 ± 1	34 ± 2
52	Pyr-R-P-R-L-S-H-K-G-P-Nle-**1Nal-Tcc**-OH	1.01 ± 0.43	6.0 ± 0.8	25 ± 1	96 ± 6
53	Pyr-R-P-R-L-S-H-K-G-P-Nle-**1Nal-Db$_z$g**-OH	0.08 ± 0.01	3.8 ± 0.9	2.8 ± 0.1	36 ± 1
54	Pyr-R-P-R-L-S-H-K-G-P-Nle-**1Nal-dcypTyr(OH)**-OH	1.1 ± 0.1	10 ± 2	178 ± 13	95 ± 14

[a] K_i was calculated from experimental IC_{50} values (the concentration of ligand that displaces 50% of radiolabeled [^{125}I][Nle^{75}, Tyr^{77}]Pyr-apelin-13) using the Cheng−Prusoff equation.[69] Values represent the mean ± SEM of two to three experiments, each performed in duplicate. [b] EC_{50} corresponds to the concentration of ligand that produces 50% dissociation of Gα_{i1} from the G$\beta\gamma$ subunits. [c] EC_{50} corresponds to the concentration of ligand that produces 50% recruitment of the Gα_{12} effector (PDZ-RhoGEF) to the cell membrane. [d] EC_{50} is the concentration of ligand that produces 50% recruitment of β-arrestin2 to the apelin receptor. Values represent the mean ± SEM of three experiments, each performed in triplicate. [e] Not tested yet.

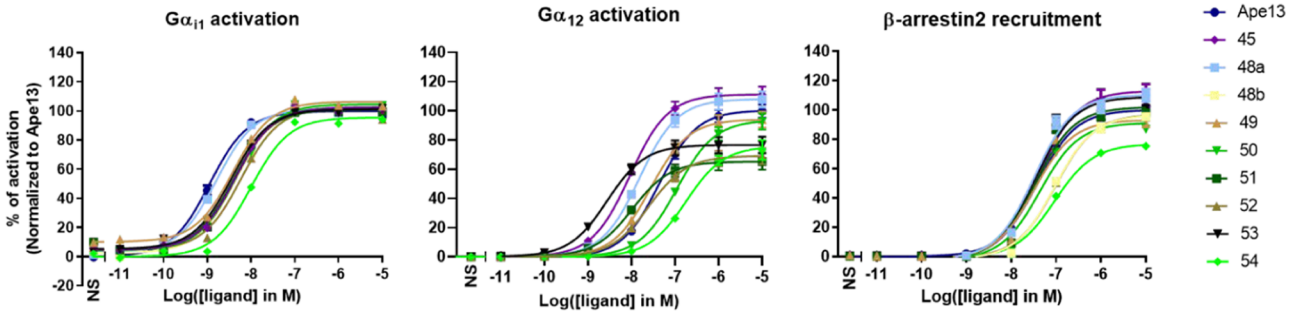

Figure 9. BRET dose−response curves of Gα_{i1}, Gα_{12}, and β-arrestin2 pathways of Ape13 analogues with combined modification on Pro12 and Phe13.

opposed to the other analogues (Figure 5), suggesting that the high-affinity complex of **41** with the apelin receptor may not efficiently trigger Gα_{12} activation. Interestingly though, **41** remains a full agonist, having similar potency as Ape13 on the Gα_{i1} and β-arrestin2 pathways (Figure 5). Regarding β-arrestin2 recruitment, the bulky dcypTyr(OBn) and dcypTyr-(OH) substitutions elicit lower potencies (**36**, β-arr2 EC_{50} 367 nM; **37** EC_{50} 361 nM vs Ape13, EC_{50} 40 nM) and analogue **36** behaves as a partial agonist on the β-arrestin2 pathway, producing only half of E_{max} at the highest concentration (Figure 5).

To summarize, most substitutions of Tyr(OBn) did not further improve the binding and signaling profiles of analogue **33**, except for L/D-α-MeTyr(OBn). Those results follow the same trend observed in Phe13 modifications, highlighting the advantage of α,α-disubstituted analogues at the C-terminal position of Ape13. Of particular interest, **41** emerges as a partial agonist on the Gα_{12} pathway and **36** for the β-arrestin2 pathway.

Impact of Modifications on Pro12. The Pro12 position has been studied previously using proline mimetics,[58] which improved both stability and affinity. The X-ray structure of APJ complexes with apelin-17 analogues reveals that the Pro12 residue is surrounded by a hydrophobic environment with available space for structural derivatization (Figure 1S, Supporting Information).[70] For this reason, we substituted Pro12 with bulky proline derivatives (e.g., Hyp(4-OBn), P3cPhe, Tic) and aromatic residues (e.g., 1-Nal, Trp) (Figure 6 and Table 3). Binding results confirm that the Pro binding pocket is large and can accommodate bulky residues without major loss in receptor binding affinity (e.g., Hyp(4-OBn), **42**, K_i 2.1 nM vs Ape13, K_i 0.7 nM). However, side-chain-constrained residues, such as P3cPhe and Tic, may impact the peptide backbone conformation since these substitutions result in 6- to 14-fold loss in affinity, respectively (**43**, K_i 4.2 nM; **44**,

https://dx.doi.org/10.1021/acs.jmedchem.0c01941
J. Med. Chem. 2021, 64, 5345−5364

K_i 9.7 nM). Surprisingly, replacement of Pro12 with an unconstrained aromatic amino acid (1-Nal and Trp) leads to a significant improvement in binding affinity (**45**, K_i 0.12 nM; **46**, K_i 0.18 nM). Aia substitution also follows the same trend, further improving affinity (**47**, K_i 0.08 nM).

Regarding signaling, compounds **43** and **44** having the proline analogue Pc3Phe or constraint residue Tic substitution display 9- to 17-fold loss in the $G\alpha_{i1}$ pathways and 3- to 11-fold loss in β-arrestin recruitment, while the $G\alpha_{12}$ pathway remains comparable to the endogenous ligand (Figure 7). In contrast, compound **45** (Pro12 → 1Nal, EC_{50} $G\alpha_{12}$ 9.2 nM) or **47** (Pro12-Phe13 → Aia-Phe, EC_{50} $G\alpha_{12}$ 11 nM) is comparable on $G\alpha_{i1}$ activation and β-arrestin recruitment compared to Ape13 but fourfold more potent on the $G\alpha_{12}$ pathway (Ape13, EC_{50} $G\alpha_{12}$ 43 nM). These results suggest that proline is not mandatory for this position and aromatic residues, such as 1Nal or Aia, could be a favorable replacement. This is consistent with the presence of a hydrophobic and aromatic environment around position Pro12 in the APJ binding pocket.

Impact of Combined Modifications of Pro12 and Phe13. The 1Nal substitution of Pro12 shows a great benefit for binding affinity as well as signaling potency. Indeed, **45** (Pro12 → 1Nal) possesses an excellent binding affinity (**45**, K_i 0.12 nM) and high potency across the different signaling pathways tested. In contrast with Aia, this residue was easily incorporated with other constrained amino acids at the Phe13 position. For this reason, **45** was chosen as a starting point for further modifications to test the potential for additive or synergistic effects (Figure 8 and Table 4). The results show that the combined modifications between 1-Nal at Pro12 and Tic (**48a**, K_i 0.09 nM) and D-Tic (**49**, K_i 0.08 nM) at Phe13 are beneficial, leading to compounds with sub-nM affinities. The affinity contribution of 1-Nal at the Pro12 position seems pivotal when Tic (**48a**) and D-Tic (**49**) residues are placed in the Phe13 position, as the latter no longer influence the binding constant (cf. compounds **25** and **26**, Table 1). Remarkably, replacement of 1-Nal by its regioisomer 2-Nal nullifies improvements in binding affinity (**48b**, K_i 0.37 nM vs **48a**, K_i 0.09 nM), again confirming the beneficial role of the 1-Nal residue. Introduction of a methyl substituent at the β-position of Tic reduces the affinity by two- to fivefold (**50**, K_i 0.40 nM; **51**, K_i 0.16 nM). This result may be explained by the proximity of β-methyl substitution on Tic residues to the C-terminal carboxylate group, hindering its interaction with Lys268 or Arg168 of APJ.[70] While the C-terminal carboxylate is important for binding, such steric hindrance could be detrimental.[13] The combination of 1-Nal and Db_zg generated compound **53** (K_i 0.08 nM), which is as potent as the previous analogue containing Db_zg (i.e., **5**, K_i 0.04 nM), confirming the consistent benefit of α,α-disubstitution at the level of Phe13. As a key residue, Fmoc-Db_zg-OH could be easily obtained from ethyl 2-nitroacetate through a four-step synthesis (Scheme 4).

Improvements in binding affinity do not necessarily translate into improvements in signaling potency (Table 4 and Figure 9). For analogues **48a**−**54**, they manifest similar or slightly lower potency on the $G\alpha_{i1}$ pathway (EC_{50} 1.6−10 nM) and the β-arrestin recruitment (EC_{50} 32−95 nM) compared to Ape13 (EC_{50} $G\alpha_{i1}$ 1.1 nM, EC_{50} β-arr2 40 nM). The most significant change in $G\alpha_{12}$ activation was observed with several potent analogues, such as **48a** (bearing 1Nal-Tic), **51** (1Nal-(β-diMeTic)), and **53** (1Nal-Db_zg), which display 3−15-fold potency increases (EC_{50} 2.8−10 nM vs Ape13 EC_{50} $G\alpha_{i1}$ 43 nM). Among these, **53** (K_i 0.08 nM, Pro12-Phe13 → 1Nal-Db_zg) possesses the highest potency on the $G\alpha_{12}$ pathway (EC_{50} $G\alpha_{12}$ 2.8 nM), becoming the most potent $G\alpha_{12}$ activator known to date of the Ape13-modified analogues.

Scheme 4. Synthesis of Fmoc-α,α-dibenzylglycine[a]

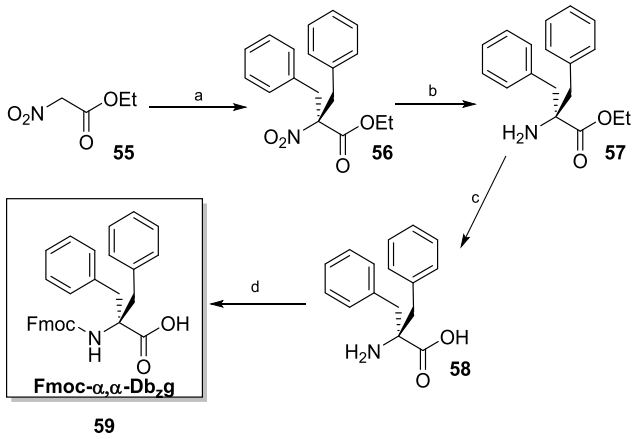

[a](a) BnBr, *N*,*N*-diisopropylethylamine (DIPEA), TBAI, dry *N*,*N*-dimethylformamide (DMF), 0−25 °C, ovn, 35%; (b) Zn, trace HCl 1 M, AcOH, rt, 2 h, 70%; (c) KOH 2 M, EtOH, reflux, 2 h, 90%; (d) (i), TMSCl, DIPEA, DCM, rt, 10 min; (ii), Fmoc-Cl, DCM, rt, ovn, 73% over two steps.

***In Vitro* Stability in Rat Plasma and ACE2 Degradation.** Analogues with high affinity for the apelin receptor were assessed for their *in vitro* stability in rat plasma (Table 5).

Table 5. Stability of Ape13 Analogues in Rat Plasma

	peptide sequence	rat plasma $t_{1/2}$ (h)[a]
Ape13	Pyr-R-P-R-L-S-H-K-G-P-M-P-F	0.5 ± 0.1
25	Pyr-R-P-R-L-S-H-K-G-P-Nle-P-Tic-OH	1.3 ± 0.1
26	Pyr-R-P-R-L-S-H-K-G-P-Nle-P-(d-Tic)-OH	0.8 ± 0.2
27	Pyr-R-P-R-L-S-H-K-G-P-Nle-P-Db_zg-OH	0.5 ± 0.1
41	Pyr-R-P-R-L-S-H-K-G-P-Nle-P-(d-α-MeTyr(OBn))-OH	0.9 ± 0.3
45	Pyr-R-P-R-L-S-H-K-G-P-Nle-1Nal-F-OH	0.4 ± 0.1
46	Pyr-R-P-R-L-S-H-K-G-P-Nle-W-F-OH	0.2 ± 0.1
47	Pyr-R-P-R-L-S-H-K-G-P-Nle-(Aia)-F-OH	5.8 ± 1.6
48a	Pyr-R-P-R-L-S-H-K-G-P-Nle-1Nal-Tic-OH	3.4 ± 0.3
49	Pyr-R-P-R-L-S-H-K-G-P-Nle-1Nal-(d-Tic)-OH	6.1 ± 1.2
50	Pyr-R-P-R-L-S-H-K-G-P-Nle-1Nal-(β-MeTic)-OH	5.3 ± 0.5
51	Pyr-R-P-R-L-S-H-K-G-P-Nle-1Nal-(β-diMeTic)-OH	6.3 ± 2.1
52	Pyr-R-P-R-L-S-H-K-G-P-Nle-1Nal-Tcc-OH	7.8 ± 0.9
53	Pyr-R-P-R-L-S-H-K-G-P-Nle-1Nal-Db_zg-OH	7.3 ± 1.1
54	Pyr-R-P-R-L-S-H-K-G-P-Nle-1Nal-dcypTyr(OH)-OH	>24 h

[a]Values represent the mean ± SEM of three determinations. The most abundant fragments detected at the time point near $t_{1/2}$ are underlined.

Among them, the two most promising compounds (**47**, **53**) were additionally tested for their stability against recombinant rat ACE2 compared with **46** and Ape13. Indeed, the fact that Ape13 is cleaved between Pro12 and Phe13 by ACE2 and PRCP proteases[46,47] suggests that modifying either residue could improve resistance to proteolysis. Single modification on

https://dx.doi.org/10.1021/acs.jmedchem.0c01941
J. Med. Chem. 2021, 64, 5345−5364

Phe13 slightly increases plasma stability, in agreement with previous findings (**25**, $t_{1/2}$ 1.3 h; **26**, $t_{1/2}$ 0.8 h vs Ape13, $t_{1/2}$ 0.5 h).[43] Regarding Pro12, substitution with 1-Nal or Trp does not change the half-life (**45**, $t_{1/2}$ 0.4 h; **46**, $t_{1/2}$ 0.2 h). The analogue with Pro12 → Trp substitution (**46**) showed some level of resistance to ACE2, whereas Ape13 was rapidly cleaved (Figure 10). However, the cleavage of **46** by ACE2 was still

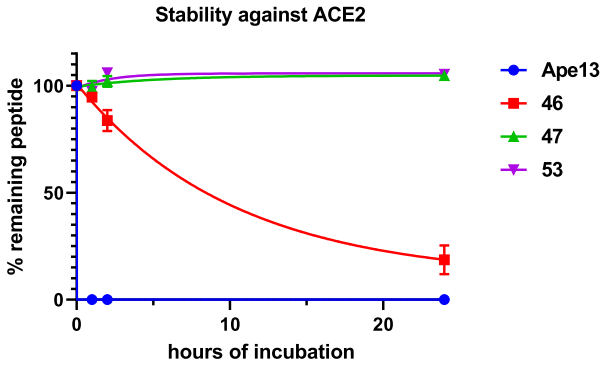

Figure 10. Stability of analogues **46**, **47**, and **53** against rat ACE2 cleavage, compared to Pyr-apelin-13. The Ape13 analogues (final concentration 50 μM) were incubated with 20 nM enzyme (n = 3).

clearly observed at 24 h. The consensus recognition sequence of this enzyme is Pro-X-Pro-hydrophobic, yet several exceptions have been reported.[46] Moreover, this analogue could be targeted by other proteases, indicating that single mutation in the sequence may not be sufficient to protect the peptide against enzymatic degradation. When the peptide bond between Pro12 and Phe13 of apelin is prone to proteolysis, constraining this particular bond represents an elegant way to improve stability. Consequently, the side-chain-constrained version of analogue **46** was prepared (with Aia-Phe, **47**, K_i 0.08 nM), showing an excellent binding affinity and a great improvement in plasma stability (**47**, $t_{1/2}$ 5.8 h vs Ape13, $t_{1/2}$ 0.5 h). As expected, **47** also displayed complete resistance against ACE2 cleavage after 24 h (Figure 10).

The combined modification of Pro12 and Phe13 provides improved peptide resistance to proteolytic degradation. All compounds with double modifications (**48a** to **54**; $t_{1/2}$ 3.4 to >24 h) consistently display higher half-lives compared to those with single modifications (**25**−**27**, **45**, **46**; $t_{1/2}$ 0.2−1.3 h), except for analogue **47**.

The cleavage fragments were detected by comparing MS spectra between 0 h and the time point near the half-life of the compound. By confirming the presence of those fragments, we identified several cleavage sites, such as the Leu5-Ser6 peptide bond (attributed to neprilysin)[48] and the Ser6-His7 one for analogues possessing Phe13 substitution (**25**, **26**, **27**, Table 5). Regarding Pro12-substituted analogues, the dominant cleavage site is between Nle11-1Nal and Nle11-Trp12 (**45**, **46**, Table 5). The C-terminal fragments were usually detected as the remaining part for compounds with significantly improved half-lives (**47**, **49**−**54**), whereas *N*-terminal fragments remained dominantly present for analogues with lower half-lives (Ape13, **25**, **45**, **46**). These results suggest that stabilizing the C-terminal end of apelin-13 improves peptide stability, in agreement with previous studies.[37]

In this series, **53** is the overall lead in terms of receptor binding (**53**, K_i 0.08 nM vs Ape13, K_i 0.7 nM) and signaling potency (**53**, Gα_{12} EC_{50} 2.8 nM vs Ape13, EC_{50} 43 nM), as well as complete resistance to ACE2 cleavage (Figure 10) and high stability against plasma proteases, with an *in vitro* half-life of 7.3 h.

***In Vivo* Pharmacokinetics in Rats.** The two most promising apelin analogues in this series, i.e., **47** (K_i 0.08 nM, $t_{1/2}$ 5.8 h) and **53** (K_i 0.08 nM, $t_{1/2}$ 7.3 h), were selected for *in vivo* pharmacokinetics in rats (Figure 11). In these

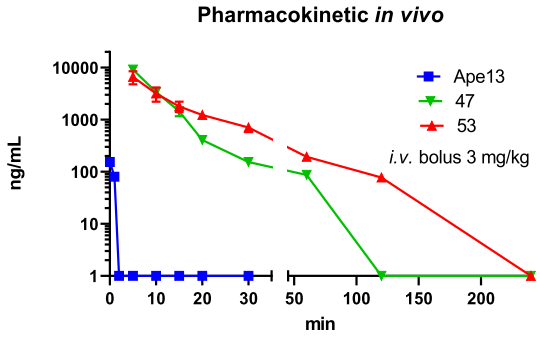

Figure 11. Trace of the plasma concentration for compounds **47**, **53**, and Ape13 in male Sprague−Dawley rats (n = 3).

experiments, animals received the test compounds at a dose of 3 mg/kg *i.v.* The plasma concentration of these compounds was monitored at 5, 10, 15, 20, 30, 60, 120, and 240 min after injection by liquid chromatography and tandem mass spectrometry (LC-MS/MS) analysis. Results show that analogues **47** and **53** are definitely more stable than Ape13, displaying half-lives of 20−26 min *in vivo* (compared to <1 min for Ape13) and significant improvement in target exposure (AUC 0.12−0.13 mg*(min/mL) vs AUC 0.24.10^{-3} mg*(min/mL) of Ape13). The clearance of these analogues is medium, with values around 23−27 mL/(min kg), yet shows drastic improvements compared to Ape13. In conclusion, these results confirm that Pyr-apelin-13 analogues **47** and **53** are not only more stable in the rat plasma *in vitro* assay but also possess improved pharmacokinetic profiles *in vivo* (Table 6).

Table 6. *In Vivo* Pharmacokinetic Parameters for Compounds 47, 53, and Ape13 in Male Sprague−Dawley Rats (n = 3)[a]

compounds	AUC_{tot} min*(mg/mL)	$t_{1/2}$ (min)	clearance mL/(kg min)
47	0.13 ± 0.01	20 ± 1	23 ± 2
53	0.12 ± 0.03	26 ± 1	27 ± 7
Ape13	0.0002 ± 0.0001	<1 min	>100

[a]Analogues were administered by *i.v.* bolus injection at 3 mg/kg.

***In Vivo* Blood Pressure Measurement.** Finally, to compare *in vivo* effects of modified analogues with Ape13, compounds **36**, **41**, **47**, and **53** were administered *i.v.* to rats at a dose of 19.6 nmol/kg while the mean arterial blood pressure (MABP) was monitored (Figure 12). Ape13 is known to induce a blood pressure drop following an *i.v.* bolus that reaches the maximum effect at the tested dose.[71] Analogues **41**, **47**, and **53** produced a similar blood pressure drop as Ape13 (around −30 mmHg after 1 min), confirming that the compounds are active *in vivo*. In contrast, analogue **36** has no effect on blood pressure, even with a higher dose (65 nmol/kg). Since the hypotensive effect of activated APJ is correlated with the recruitment of β-arrestins,[36] those results might be explained by the fact that analogues **41**, **47**, and **53** have

https://dx.doi.org/10.1021/acs.jmedchem.0c01941
J. Med. Chem. 2021, 64, 5345−5364

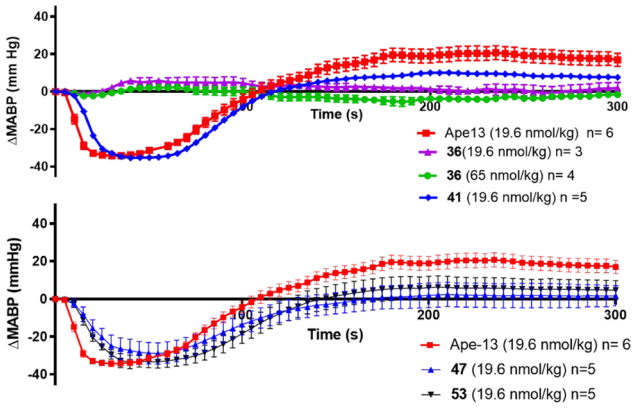

Figure 12. Tracing of blood pressure variation of male Sprague–Dawley rats after administration of compounds **47**, **53**, and Ape13 at 19.6 nmol/kg (n = 5).

comparable potencies and efficacies for the recruitment of β-arrestin2 as Ape13 (similar EC_{50} values and E_{max}), while **36** is only a partial agonist (E_{max} 53%) and possesses ~10-fold lower potency on this pathway compared to other analogues. On the other hand, a partial agonist on the $G\alpha_{12}$ pathway such as **41** produces an effect on blood pressure, suggesting that this pathway may not be responsible for the vasodilator effect of apelin. Although **47** and **53** possess much higher half-lives and exposure *in vivo* than Ape13, their effects on blood pressure are only marginally longer (130–150 vs 100 s to normalization of blood pressure), testifying the efficiency of the baroreflex[72] to counteract the hypotensive effect of systemically administered apelin agonists.

CONCLUSIONS

The C-terminus of Ape13 was previously suggested to represent a crucial site to modulate the signaling of APJ.[37,42] In this work, the Pro12 and Phe13 of Ape13 were modified using a series of side-chain-constrained residues, which extends SAR knowledge of this bioactive peptide. Careful modifications with the help of >30 derivatives led to significant improvements not only in binding affinity but also in terms of signaling profiles and stability. As such, single modifications of Pro12 with 1-Nal, Trp, or Aia increased affinity and potency on the $G\alpha_{12}$ pathway, while substitution of Phe13 with Db_zg, D-α-MeTyr(OBn), or D-Tic improved potency for both the $G\alpha_{12}$ and β-arrestin2 pathways, providing one of the most potent Ape13 analogues on β-arrestin2 recruitment (**27**, EC_{50} 10 nM). Several analogues possess sub-nM affinity (40–90 pM); among them, compound **27** bearing Db_zg (K_i 40 pM) displays the highest affinity in this series. The peptide bond between Pro12 and Phe13 is known to be cleaved by ACE2 and by PRCP.[46,47] Single modification of the C-terminal residues provides limited protection of the apelin peptide against proteolytic degradation. In contrast, the combined modifications of Pro12 and Phe13 or constraining the cleaved bond in a dipeptide moiety (e.g., **47**, Aia-Phe, K_i 0.08 nM) dramatically increases stability in rat plasma. The resulting analogues show a half-life ranging from 3 to 7 h. The combined modifications also result in the most potent $G\alpha_{12}$ agonist in this series, with a 15-fold improvement (**53**, K_i 0.08 nM, EC_{50} $G\alpha_{12}$ 2.8 nM) compared to the endogenous ligand (Ape13, K_i 0.7 nM, EC_{50} $G\alpha_{12}$ 43 nM), as well as partial agonists of the $G\alpha_{12}$ (**41**, E_{max} 46%) and the β-arrestin (**36**, E_{max} 53%) pathway. The pharmacokinetic profiles of the two most promising analogues **47** (Aia-Phe) and **53** (Db_zg) were characterized, showing half-lives *in vivo* of around 20–26 min (>15-fold improvement compared to Ape13) and complete resistance to ACE2 cleavage. Those stable and refined analogues, along with those possessing diverse signaling pathways, represent unique tools to further unravel the pharmacology of the apelinergic system.

EXPERIMENTAL SECTION

Synthetic Procedures and Compound Characterization (Solution-Phase Synthesis). Thin-layer chromatography (TLC) was performed on glass plates precoated with silica gel 60F254 (Merck, Darmstadt, Germany) using the mentioned solvent systems. Visualization of the products on TLC plates was realized using UV light (254 nm) and $KMnO_4$ spray. Purification of organic molecules was performed via silica gel column chromatography (Davisil LC60A or SiliCycle SILIAFLASH P60, 40–63 μm) on a Biotage Isolera One system (Charlotte, North Carolina). Mass spectrometry (MS) was performed on a Micromass Q-Tof Micro spectrometer with electrospray ionization (ESI). High-resolution electrospray mass spectroscopy (HRMS) data were recorded with a Micromass QTOFmicro system or a maXis ESI-Q-Tof apparatus (Billerica). Analytical reversed-phase high-performance liquid chromatography (RP-HPLC) was performed using a Chromaster system (VWR Hitachi) or ultrahigh-performance liquid chromatography (UPLC)-MS system from Waters. Data collection and spectrum analysis were done with Masslynx software. Preparative RP-HPLC purification was done on a Gilson (Middleton, WI) HPLC system or a preparative HPLC from Waters (Milford) (detail in Supporting Information). All fractions were lyophilized using a Flexy-Dry lyophilizer (FTS Systems, Warminster, PA). ^1H and ^{13}C NMR spectra (298 K) were recorded at 250 and 63 MHz on a Bruker Avance DRX 250 spectrometer, at 400 and 100 MHz, respectively, on Bruker Ascend 400 or at 500 MHz and 126 MHz, respectively, on a Bruker Avance II 500 spectrometer. Chemical shifts are in parts per million (ppm). Tetramethylsilane (TMS) or residual solvent signals were used as internal standards. The solvent used is mentioned in all cases, and the abbreviations used are as follows: s (singlet), br s (broad singlet), d (doublet), dd (double doublet), t (triplet), t* (pseudo triplet), q (quadruplet), and m (multiplet). The assignments were made using one-dimensional (1D) ^1H and ^{13}C spectra or two-dimensional (2D) HSQC, HMBC, and COSY spectra. All commercial reagents and solvents were used without further purification, unless otherwise stated. Solvents were dried over microwave-activated 4 Å molecular sieves, degassed with a gaseous N_2 flow, and stored under an argon atmosphere.

*β-DiMe-Pyruvic Acid (**1**).* 3-Phenylpyruvic acid (4 g, 24.4 mmol, 1 equiv) was dissolved in a mixture of THF/water (40 mL, 4:1 v/vol) solution, and the mixture was subsequently cooled by means of an ice-bath. After putting the reaction under an Ar atmosphere, methyliodide (4.5 mL, 73 mmol, 3 equiv) and an aqueous solution of NaOH (5 M, 15 mL) were added. The ice-bath was removed, and the resulting mixture was refluxed for 4 h. Additional MeI and NaOH were added after allowing the mixture to cool down to room temperature. Stirring was continued overnight at room temperature. Upon reaction completion, the mixture was concentrated *in vacuo* and redissolved in water. The aqueous phase was washed with EtOAc, acidified with an aqueous solution of HCl (1 N), and subsequently extracted with EtOAc. The combined organic layers were washed with brine, dried over $MgSO_4$, filtered, and concentrated *in vacuo*. The desired brown oil was used in the next step without purification. 89% (4.17 g); MS (ES^-): 191 $[M-H]^-$; ^1H NMR ($CDCl_3$, 250 MHz): δ (ppm) = 10.6 (br. s, 1H), 7.33–7.23 (m, 5H), 1.59 (s, 6H); ^{13}C NMR ($CDCl_3$, 63 MHz): δ (ppm) = 197.5, 162.0, 141.4, 128.9, 127.4, 126.0, 50.1, 25.2.

*β-DiMe-pyruvic Methyl Ester (**2**).* Thionylchloride (5 mL, 69 mmol, 6.6 equiv) was added dropwise to a solution of 3-methyl-2-oxo-3-phenylbutanoic acid (2 g, 10.4 mmol, 1 equiv) in dry methanol (52 mL), which was cooled by means of an ice-bath. After completing the addition, the mixture was heated to reflux and stirring was continued

https://dx.doi.org/10.1021/acs.jmedchem.0c01941
J. Med. Chem. 2021, 64, 5345–5364

overnight. The volatiles were removed under reduced pressure. No additional washings or purifications were performed, and the brown oil was used in the next step without purification. 90% (1.93 g); MS(ES^+): no ionization observed; ^{1}H NMR ($CDCl_3$, 250 MHz): δ (ppm) = 7.38−7.24 (m, 5H); 3.59 (s, 3H), 1.62 (s, 6H); ^{13}C NMR ($CDCl_3$, 63 MHz): δ (ppm) = 197.88, 162.55, 141.78, 128.77, 127.30, 126.18, 52.22, 50.48, 25.19.

*Methyl (E)-2-(Hydroxyimino)-3-methyl-3-phenylbutanoate (**3**).* Methyl 3-methyl-2-oxo-3-phenylbutanoate (1 g, 4.84 mmol, 1 equiv) was dissolved in dry methanol (18 mL), followed by the addition of hydroxylamine hydrochloride (1 g, 14.5 mmol, 3 equiv). The mixture was refluxed for 16 h. Upon reaction completion, the volatiles were removed *in vacuo*. The residue was redissolved in EtOAc and washed with brine, dried over $MgSO_4$, and filtered to yield the desired oxime. The brown oil was used in the following step without any purification. 94% (1 g); MS(ES+): 243 $[M + Na]^+$, ^{1}H NMR ($CDCl_3$, 250 MHz): δ (ppm) = 8.83 (s, 1H), 7.37−7.25 (m, 5H), 3.62 (s, 3H), 1.59 (s, 6H); ^{13}C NMR ($CDCl_3$, 63 MHz): δ (ppm) = 163.94, 158.81, 143.89, 128.31, 126.86, 126.32, 125.21, 51.88, 42.83, 27.05.

*HCl·H-βdiMe-L/D-Phe-OH (**4**).* The oxime (0.75 g, 4.85 mmol, 1 equiv) was dissolved in acetic acid (7.5 mL), and the mixture was allowed to cool by means of an ice-saltwater bath. An aqueous solution of H_2SO_4 (30%, 7.5 mL) was added followed by a portionwise addition of powdered zinc (0.66 g, 10.17 mmol, 3 equiv). Upon addition completion, the ice-saltwater bath was removed and the mixture stirred for 16 h at room temperature. The volatiles were removed *in vacuo* followed by extracting the aqueous solution with EtOAc. Basifying the aqueous layer with a saturated $NaHCO_3$ solution allowed extraction with EtOAc. The combined organic layers were dried over $MgSO_4$, filtered, and concentrated *in vacuo* to afford a white foam. Then, the ester (1 equiv) was dissolved in a 1 N HCl/acetone (1:1 v/v, 0.05 M) solution. The mixture was stirred for 6 h under reflux conditions in an oil bath at 90 °C. The acetone/water mixture was evaporated *in vacuo* when the reaction was complete. Compound HCl·H-βdiMe-Phe-OH was obtained as a white solid without any further purification. 65% (over two steps, 0.506 g); MS(ES^+): 194 $[M + H]^+$; ^{1}H NMR (DMSO-d_6, 250 MHz): δ (ppm) = 7.47 (m, 5H), 4.34 (s, 1H), 1.50 (s, 3H),1.46 (s, 3H); ^{13}C NMR (DMSO-d_6, 63 MHz): δ (ppm) = 169.82, 143.02, 129.20, 127.89, 126.38, 53.33, 40.05, 25.64, 22.65.

*Fmoc-βdiMe-Phe-OH (**5**).* The *N*-unprotected compound was dissolved in a water/acetone mixture (1:1, v/v, 0.1 M). Fmoc-OSu (1 equiv) and Na_2CO_3 (1.1 equiv) were added. After stirring for 3−4 h, the acetone was evaporated and the mixture was acidified with HCl (1 N) and extracted with EtOAc (3 times). The organic phases were combined, washed with brine, dried over $MgSO_4$, and concentrated *in vacuo*. The crude product was purified using automated flash chromatography (CH_2Cl_2 (1% AcOH): MeOH (1% AcOH) 0−20% gradient 30 min) and was obtained as a white solid. 76% (0.54 g); MS(ES^+): 438 $[M + Na]^+$; ^{1}H NMR ($CDCl_3$, 250 MHz): δ (ppm) = 7.76 (d, J = 7.4 Hz, 1H), 7.56−7.51 (m, 1H), 7. 42−7. 20 (m, 11H), 5.22 (d, J = 9.5 Hz, 1H), 4.58 (d, J = 9.5 Hz, 1H), 4.43 (m, 1H), 4.28 (m, 1H), 4.17 (m, 1H), 1.45 (s, 3H), 1.40 (s, 3H); ^{13}C NMR ($CDCl_3$, 63 MHz): δ (ppm) = 171.47, 155.94, 144.40, 143.78, 141.32, 128.22, 127.71, 127.06, 126.28, 125.01, 119.97, 66.98, 62.54, 51.77, 41.70, 25.43, 25.02.

HCl·H-βdiMe-L/D-Tic-OH. The phenylalanine derivative (0.5 g, 2.17 mmol, 1 equiv) was first fully dissolved in an aqueous solution of HCl (3 mL, 12 N) followed by the addition of formalin (1 mL). The mixture was refluxed for 2 h and was allowed to cool to room temperature upon completion. The formed white crystals were filtered off and used in the next reaction without further purification. 72% (0.40 g); MS(ES^+): 206 $[M + H]^+$; HRMS (ESP+): found 206.1166 m/z $[M + H]^+$, $[C_{12}H_{15}NO_2]^+$ calculated 206.1176; ^{1}H NMR (D_2O, 250 MHz): δ (ppm) = 7.56 (m, 1H), 7.39 (m, 1H), 7.29 (m, 1H), 7.18 (m, 1H), 4.40 (m, 2H), 4.15 (s, 1H), 1.61 (s, 3H), 1.33 (s, 3H); ^{13}C NMR (D_2O, 63 MHz): δ (ppm) = 170.92, 140.65, 128.88, 127.21, 126.92, 126.50, 125.70, 64.46, 44.60, 35.86, 27.40, 25.71.

*Fmoc-βdiMe-L/D-Tic-OH (**6**).* This product was synthesized following the procedure for the synthesis of Fmoc-βdiMe-Phe-OH from the unprotected amine. White solid, 71% (0.520 g); MS(ES^+): 428 $[M + H]^+$, 450 $[M + Na]^+$; HRMS (ESP^+): found 450.1661 m/z $[M + H]^+$, $[C_{27}H_{25}NO_4]^+$; calculated 450.1676; ^{1}H NMR ($CDCl_3$, 250 MHz, rotamers visible, ratio: 57/43): δ (ppm) = 7.78−7.05 (m, 12H), 4.48 (m, 6H), 1.56 (s, 1.7H), 1.48 (s, 1.3H), 1.24 (s, 1.7H), 1.14 (s, 1.3H); ^{13}C NMR ($CDCl_3$, 63 MHz): δ (ppm) = 175.67, 156.51, 155.52, 143.71, 141.39, 139.55, 138.94, 131.32, 131.11, 127.80, 127.14, 126.69, 126.05, 124.97, 124.18, 123.99, 120.01, 68.00, 67.84, 62.92, 62.67, 47.17, 45.12, 37.41, 31.05, 24.37.

*Fmoc-L-Aia-L-Phe-OH (**11b**).* This product was synthesized following the procedure for the synthesis of Fmoc-βdiMe-Phe-OH starting from the unprotected amine. White solid, 21% (0.320 g) over three steps: reductive amination/cyclization, hydrolysis, and Fmoc-protection. MS(ES^+): 586 $[M + H]^+$, 608 $[M + Na]^+$, HRMS (ESP +): found 608.2133 m/z $[M + H]^+$, $[C_{27}H_{25}NO_4Na]^+$ calculated 608.2156; ^{1}H NMR (DMSO-d_6, 500 MHz, 348.15 K, rotamers visible): δ (ppm) = 10.60 (s, 1H), 7.86−7.72 (m, 4H), 7.42−7.30 (m, 6H), 7.13−7.07 (m, 6H), 7.04−6.98 (m, 2H), 5.22 (dd, J = 8.2 Hz, J = 6.2 Hz, 1H), 4.9 (br. s, 2H), 4.41−4.31 (m, 3H), 4.25 (m, 1H), 3.29 (dd, J = 14.4 Hz, J = 6 Hz, 1H), 3.05 (m, 2H), 2.78 (ps t, J = 13.2 Hz, 1H); ^{13}C NMR (DMSO-d_6, 125 MHz, 298 K, rotamers visible): δ (ppm) = 172.56, 171.81, 155.76, 144.44, 144.24, 141.19, 137.80, 134.88, 131.68, 129.19, 128.55, 128.12, 128.00, 127.57, 126.63, 125.89, 125.81, 121.45, 120.57, 118.96, 117.89, 111.46, 107.05, 66.26, 60.01, 51.85, 47.14, 42.49, 34.92, 27.97.

*Alloc-cypTyr-OH and Alloc-dcypTyr-OH (**14a and 14b**).* L-Tyr-OH with weight 4 g was weighed in a round-bottom flask, and around 20 mL of H_3PO_4 85% (20 mL) and 4 mL of cyclopentanol were added. The mixture was stirred at 100 °C overnight. After 16 h, a small sample of the mixture was collected in a test tube, neutralized with $NaHCO_3$, derivated with a few drops of allyl chloroformate (mixed and stirred for 15 min), extracted, and analyzed using LC/MS analysis to confirm the presence of the desired product. The reaction produced a mixture of cypTyr-OH (**13a**, monoalkylation) and dcypTyr-OH (**13b**, dialkylation). For the workup, the reaction mixture was poured slowly into 100 mL of ice water and neutralized with 30 g of $NaHCO_3$ (CAUTION: vigorous reaction). A small amount of $NaHCO_3$ was added to adjust the pH of this mixture to 7, and the product was precipitated. The suspension was filtered and washed with cold water and dried under a fume hood for 1 day, obtaining 2.89 g of crude product (UPLC provided below, Figure S2). The product was used as such in the next reaction without further characterization.

The mixture of cypTyr-OH (**13a**) and dcypTyr-OH (**13b**) (2.89 g) was suspended in 40 mL of THF-H_2O (1:1, v/v), and 1.29 g of $NaHCO_3$ was added. Allyl chloroformate (1.63 mL, 1,2 equiv) was dropped slowly to the mixture for 5 min at 0 °C, and the mixture was stirred for 15 min at room temperature. After the TLC confirmed complete consumption of the starting materials, the reaction mixture was acidified with HCl (1 M) until pH 4−5 (around 20 mL). Around 30 mL of NaCl saturated solution was added, and the product was extracted with EtOAc (3 × 20 mL). The organic phases were combined, dried on $MgSO_4$, and evaporated *in vacuo* to yield the crude product. The alloc-cypTyr-OH (**14a**) and alloc-dcypTyr-OH (**14b**) were separated using flash chromatography (gradient 15−40% EtOAc in hexane + 0.25% AcOH) with a total yield of 55%. Alloc-cypTyr-OH (**14a**): HRMS: found 332.1509 $[M - H]^-$, calculated 332.1503. ^{1}H NMR ($CDCl_3$, 400 MHz, 298 K) δ (ppm) 6.96 (d, J = 1.6 Hz, 1H), 6.82 (dd, J = 8.0, 1.3 Hz, 1H), 6.64 (d, J = 8.1 Hz, 1H), 5.87 (m, 1H), 5.28 (d, J = 17.1 Hz, 1H), 5.20 (m, 2H, proton of ethylene + amide proton), 4.63 (dd, J = 13.8, 5.8 Hz, 1H), 4.56 (d, J = 5.6 Hz, 2H), 3.28−3.14 (m, 1H), 3.07 (qd, J = 14.1, 5.7 Hz, 2H), 1.99 (m, 2H), 1.84−1.42 (m, 6H); ^{13}C NMR ($CDCl_3$,101 MHz, 298 K) δ (ppm) 176.38, 155.99, 152.86, 132.53, 132.50, 128.23, 127.44, 127.35, 118.18, 115.66, 66.22, 54.78, 38.95, 37.31, 33.06, 32.99, 25.49, 25.47. Alloc-dcypTyr-OH (**14b**): HRMS: found 400.2137 $[M - H]^-$, calculated 400.2129. ^{1}H NMR ($CDCl_3$, 400 MHz, 298 K) δ (ppm): 6.82 (s, 2H), 5.88 (s, 1H), 5.28 (d, J = 17.2 Hz, 1H), 5.20 (d, J = 10.4

https://dx.doi.org/10.1021/acs.jmedchem.0c01941
J. Med. Chem. 2021, 64, 5345−5364

Hz, 1H), 5.10 (d, J = 8.1 Hz, 1H), 4.66−4.58 (m, 1H), 4.56 (d, J = 4.6 Hz, 2H), 3.22−3.00 (m, 4H), 2.08−1.93 (m, 4H), 1.85−1.48 (m, 12H); ^{13}C NMR ($CDCl_3$, 101 MHz, 298 K) δ (ppm): 177.00, 155.82, 150.64, 132.59, 131.72, 126.89, 125.15, 118.00, 66.07, 54.79, 39.11, 37.49, 33.07, 25.46, 25.44.

*Alloc-dcypTyr(OBn)-OH and Alloc-cypTyr(OBn)-OH (**15a and 15b**).* Alloc-cypTyr-OH (1.67 g, 4.76 mmol, 1 equiv) was dissolved in ACN (25 mL), and K_2CO_3 (1.98 g, 14.3 mmol, 3 equiv) was added. Benzyl bromide (1.24 mL, 10.4 mmol, 2.2 equiv) was added dropwise while stirring. The reaction mixture was heated at 90 °C for 1 h and overnight at room temperature to completely alkylate both COOH and OH functions. Once the reaction was done, solid particles (KBr, K_2CO_3) were remove by filtration and ACN was evaporated *in vacuo*. Water (around 50 mL) was added, and the product was extracted with EtOAc (50 mL). The organic phase was combined and washed with water and brine to remove residual base. The product was purified by flash chromatography (20−35% EtOAc in hexane for 10 CV) to give the intermediate Alloc-cypTyr(OBn)-OBn. HRMS: found 514.2596 $[M + H]^+$, calculated 514.2488. ^{1}H NMR ($CDCl_3$, 400 MHz, 298 K) δ (ppm): 7.48−7.27 (m, 10H), 6.99 (d, J = 1.8 Hz, 1H), 6.82 (dd, J = 8.2, 1.6 Hz, 1H), 6.77 (d, J = 8.3 Hz, 1H), 5.92 (ddd, J = 22.6, 10.8, 5.6 Hz, 1H), 5.37−5.26 (m, 1H), 5.26−5.19 (m, 2H), 5.16 (s, 2H), 5.06 (s, 2H), 4.69 (dd, J = 14.0, 5.8 Hz, 1H), 4.58 (d, J = 5.5 Hz, 2H), 3.43−3.32 (m, 1H), 3.09 (d, J = 5.8 Hz, 2H), 2.05−1.96 (m, 2H), 1.82−1.72 (m, 2H), 1.72−1.62 (m, 2H), 1.61−1.50 (m, 2H). ^{13}C NMR ($CDCl_3$,101 MHz, 298 K) δ (ppm): 171.68, 155.82, 155.60, 137.58, 135.25, 132.73, 128.68, 128.62, 128.52, 128.38, 127.96, 127.84, 127.57, 127.31, 127.22, 117.86, 111.86, 70.18, 67.20, 65.87, 55.02, 39.13, 37.67, 33.09, 33.06, 25.57. Alloc-cypTyr(OBn)-OBn (1.93 g, 3.67 mmol) was dissolved in EtOH (20 mL), and an aqueous solution of KOH (2.2 mL, 2 M) was added. In case the mixture was still transparent, more water was added until it turned cloudy. The suspension was heated to 70 °C for 15 min. The mixture was acidified with 5 mL of HCl 1 M and extracted with EtOAc. The organic phase was dried and the crude product was purified using flash chromatography (20−30% AcOEt in hexane + 0.25% AcOH in 10 CV) to obtain **15a**. Alloc-dcypTyr(OBn)-OH (**15a**): HRMS: found 422.1981 $[M - H]^-$, calculated 422.1973. ^{1}H NMR ($CDCl_3$, 400 MHz, 298 K) δ (ppm): 7.46−7.29 (m, 5H), 7.04 (d, J = 1.1 Hz, 1H), 6.94 (dd, J = 8.3, 2.0 Hz, 1H), 6.83 (d, J = 8.3 Hz, 1H), 5.90 (ddd, J = 22.6, 10.8, 5.6 Hz, 1H), 5.35−5.11 (m, 3H), 5.05 (s, 2H), 4.65 (dd, J = 13.6, 5.9 Hz, 1H), 4.57 (d, J = 5.4 Hz, 2H), 3.46−3.33 (m, 1H), 3.15 (dd, J = 14.0, 5.4 Hz, 1H), 3.07 (dd, J = 14.1, 6.2 Hz, 1H), 2.06−1.96 (m, 2H), 1.81−1.50 (m, 6H). ^{13}C NMR ($CDCl_3$, 101 MHz, 298 K) δ (ppm): 176.94, 155.90, 155.86, 137.55, 135.47, 132.58, 128.64, 128.02, 127.86, 127.45, 127.27 (peak overlap), 118.06, 111.95, 70.22, 66.10, 54.78, 39.08, 37.23, 33.10, 25.60 (25.59). The same protocol was used for synthesis of Alloc-dcypTyr(OBn)-OH (**15b**): HRMS: found 492.2758 $[M + H]^+$, calculated 492.2745. ^{1}H NMR ($CDCl_3$, 400 MHz, 298 K) δ (ppm): 7.36−7.13 (m, 5H), 6.75 (s, 2H), 5.74 (ddd, J = 22.4, 10.8, 5.6 Hz, 1H), 5.25−4.89 (m, 3H), 4.65 (s, 2H), 4.58−4.45 (m, 1H), 4.42 (d, J = 1.4 Hz, 2H), 3.33−3.14 (m, 2H), 3.02 (dd, J = 14.0, 5.3 Hz, 1H), 2.93 (dd, J = 14.0, 6.2 Hz, 1H), 1.94−1.80 (m, J = 13.0, 11.5, 5.7 Hz, 4H), 1.72−1.58 (m, 4H), 1.56−1.44 (m, 4H), 1.44−1.30 (m, 4H). ^{13}C NMR ($CDCl_3$,101 MHz, 298 K) δ (ppm): 177.26, 156.07, 154.43, 140.36, 138.14, 132.87, 131.74, 128.99, 128.37, 127.87, 126.07, 118.35, 76.92, 66.41, 54.96, 38.71, 38.04, 35.73, 35.71, 26.35.

*Synthesis of (3-(4-(Benzyloxy)phenyl)prop-1-ynyl)trimethylsilane (**17a**).* To a stirred solution of 4-benzyloxybenzyl chloride (3.05 g, 1.0 equiv, 13.11 mmol) in dry acetonitrile (0.15 M, 87 mL) at room temperature under argon, purified CuI (2.5 g, 1.0 equiv, 13.11 mmol) was added, followed by K_2CO_3 (3.62 g, 2.0 equiv, 26.21 mmol) and tetrabutylammonium iodide (4.84 g, 1.0 equiv, 13.11 mmol). After 5 min of stirring, ethynyltrimethylsilane (2.22 mL, 1.2 equiv, 15.75 mmol) was added dropwise as a neat liquid and the mixture was stirred at 40 °C for 24 h. The reaction mixture was diluted with a saturated ammonium chloride solution (50 mL) and extracted with diethyl ether (3 × 50 mL). The organic phase was dried over $MgSO_4$, filtered, and concentrated under reduced pressure. The crude product was purified by silica gel flash column chromatography using EtOAc-hexane (1: 9, v/v) as the eluant to afford the desired product as a colorless oil. Yield: 94% (3.61 g); chemical formula: $C_{19}H_{22}OSi$; MW: 294.4690 g/mol; HRMS m/z: $[M + Na]^+$ calculated for $C_{19}H_{22}OSi$ 294.1440, found 294.1427; ^{1}H NMR (300 MHz, $CDCl_3$) δ (ppm) 7.46−7.30 (m, 5H), 7.25 (d, J = 8.8 Hz, 2H), 6.94 (dt, J = 8.7, 3 Hz, 2H), 5.06 (s, 2H), 3.60 (s, 2H), 0.19 (t, J = 3.6 Hz, 9H). ^{13}C NMR (300 MHz, $CDCl_3$) δ (ppm) 157.65, 137.19, 128.95, 128.73, 128.66, 128.00, 127.52, 114.97, 104.88, 86.67, 70.10, 25.43, 0.26.

*1-(Benzyloxy)-4-(prop-2-ynyl)benzene (**17b**).* To a stirred solution of (3-(4-(benzyloxy)phenyl)prop-1-ynyl)trimethylsilane (1.6 g, 1.0 equiv, 5.43 mol) in dry THF (0.09 M, 32 mL) and methanol (0.09 M, 32 mL) was added anhydrous K_2CO_3 (3.83 g, 5.1 equiv, 27.71 mmol). Stirring was continued at room temperature for 1.5 h. The solvent was removed under reduced pressure, and the residue was extracted with diethyl ether (3 × 50 mL). The organic extract was washed with brine (75 mL), dried over $MgSO_4$, filtered, and concentrated under reduced pressure. The crude product was purified by silica gel flash column chromatography using EtOAc-hexanes (2:98, v/v) as eluents to afford **17b** as a white solid in 88% (1.06 g) yield. The product was used as such in the next reaction without further characterization.

*(S,E)-4-(4-(Benzyloxy)phenyl)-1-((1R,2S,5R)-2-isopropyl-5-methylcyclohexyl)-3-methylbut-2-en-1-ol (**18**).* To a stirred suspension of bis-(cyclopentadienyl) zirconium(IV) dichloride (0.61 g, 0.22 equiv, 2.08 mmol) in dry DCM (0.22 M, 33 mL) at 0 °C under argon was added dropwise a solution of trimethyl aluminum (2 M in toluene, 14.7 mL, 3.1 equiv, 29.3 mmol), and the solution was stirred for 15 min. A solution of alkyne (2.1 g, 1.0 equiv, 9.45 mmol) in DCM (10 mL) was added dropwise; the reaction mixture was stirred at room temperature for 16 h and then cooled to −78 °C before a solution of freshly distilled *p*-menthane-3-carboxaldehyde, synthesis described in Supporting Information, (2.07 g, 1.3 equiv, 12.28 mmol) in THF (0.4 M, 24 mL) was added dropwise. The reaction mixture was stirred at the same temperature for 2 h and then allowed to return to room temperature. The reaction mixture was cooled to 0 °C and quenched with a cold K_2CO_3 0.5 M solution (80 mL). The phases were separated, and the aqueous phase was extracted with Et_2O (3 × 70 mL). All organic phases were combined and washed with brine, dried over $MgSO_4$, filtered, and concentrated under reduced pressure. The crude compound was purified by flash chromatography using EtOAc:hexane (4:96 to 20:80% in 10 CV) as the eluant to afford the desired compound **18** as a colorless oil (1.79 g, 47% yield), (<5% of the other diastereomer by ^{1}H NMR). Yield: 47% (1.79 g); chemical formula: $C_{28}H_{38}O_2$; MW: 406.61 g/mol; HRMS m/z: $[M + Na]^+$ calculated for $C_{28}H_{38}O_2$: 406.2872, found 406.2868; ^{1}H NMR ($CDCl_3$, 300 MHz, 298 K) δ (ppm) 7.45−7.26 (m, 5H), 7.09 (d, J = 8,64 Hz, 2H), 6.90 (d, J = 9 Hz, 2H), 5.43 (dd, J = 8.07, 1.14 Hz, 1H), 5.05 (s, 2H), 4.68 (d, J = 8.07 Hz, 1H), 3.26 (s, 2H), 2.16 (m, 1H), 1.92 (m, 1H), 1.75−1.63 (m, 2H), 1.60 (d, J = 1.15 Hz, 3H), 1.35−1.27 (m, 3H), 1.26 (t, J = 7.2 Hz, 1H), 0.98−0.86 (m, 9H), 0.78 (d, J = 6.91 Hz, 3H); ^{13}C NMR ($CDCl_3$, 300 MHz, 298 K) δ (ppm) 157.4, 137.29, 136.27, 132.18, 129.90, 128.92, 128.64, 127.98, 127.56, 114.81, 70.15, 67.97, 45.53, 45.08, 43.26, 35.26, 34.29, 32.95, 26.45, 24.38, 23.06, 21.75, 16.41, 15.69.

*(S,E)-4-(4-(Benzyloxy)phenyl)-1-((1R,2S,5R)-2-isopropyl-5-methylcyclohexyl)-3-methylbut-2-enyl Carbamate (**19**).* To a stirred solution of alcohol (1.9 g, 1.0 equiv, 4.67 mmol) in DCM (0.12 M, 40 mL) at 0 °C under argon was added dropwise trichloroacetyl isocyanate (2.64 g, 3.0 equiv, 14 mmol), and the solution was stirred for 1 h at 0 °C (consumption of the alcohol was monitored by TLC). The solvent was evaporated under reduced pressure, and the crude intermediate was dissolved in methanol (0.15 M, 31 mL) and water (0.8 M, 16 mL) followed by addition of potassium carbonate (1.94 g, 3.0 eq, 14 mmol) at 0 °C. The reaction mixture was then stirred at room temperature overnight (∼16 h). Methanol from the reaction mixture was evaporated, and the aqueous phase was extracted with DCM (3 × 50 mL). The combined organic phases were washed with brine (70 mL), dried over anhydrous $MgSO_4$, filtered, and concentrated under reduced pressure. The crude compound was purified by silica gel flash chromatography with EtOAc-hexanes (5:95

https://dx.doi.org/10.1021/acs.jmedchem.0c01941
J. Med. Chem. 2021, 64, 5345−5364

to 20:80) as eluants to afford the desired compound **19** as a colorless oil.

*(S,E)-4-(4-(Benzyloxy)phenyl)-1-((R,E)-2-isocyanato-4-((1S,2S,5R)-2-isopropyl-5-methylcyclo hexyl)-2-methylbut-3-enyl)-benzene (**20**).* To a stirred solution of carbamate **19** (1.5 g, 1.0 equiv, 3.34 mmol) in CH_2Cl_2 (0.13 M, 26 mL) at 0 °C under argon was added triethylamine (1.39 mL, 3.0 equiv, 10 mmol) followed by dropwise addition of trifluoroacetic anhydride (0.47 mL, 1.0 equiv, 3.34 mmol) (freshly distilled over P_2O_5). The solution was stirred for 15 min at 0 °C (consumption of carbamate **19** was monitored by TLC), and then, the reaction mixture was quenched with a saturated NH_4Cl solution (50 mL). The phases were separated, and the aqueous phase was extracted with Et_2O (3 × 20 mL). The combined organic phases were washed with brine (50 mL), dried over $MgSO_4$, filtered, and concentrated under reduced pressure to afford the isocyanate as a pale-yellow oil. HRMS *m/z*: $[M + Na]^+$ calculated for $C_{29}H_{37}NO_2$: 431.2824, found 431.2814; ^1H NMR ($CDCl_3$, 300 MHz, 298 K) δ (ppm) 7.46−7.30 (m, 5H), 7.10 (d, J = 8.7 Hz, 2H), 6.91 (d, J = 8.7 Hz, 2H), 5.38 (d, J = 9.7 Hz, 1H), 5.36 (s, 1H), 5.05 (s, 2H), 2.77 (s, 2H), 1.97−1.85 (m, 1H), 1.75−1.69 (m, 2H), 1.63−1.51 (m, 2H), 1.38 (s, 3H), 1.35−1.26 (m, 1H), 1.08−0.90 (m, 4H), 0.88 (d, J = 1.90 Hz, 3H), 0.86 (d, J = 2.43 Hz, 3H), 0.70 (d, 3H, J = 6.89 Hz). ^{13}C NMR ($CDCl_3$, 300 MHz, 298 K) δ (ppm) 157.98, 137.18, 134.21, 133.00, 131.82, 128.64, 128.00, 127.58, 123.41, 114.40, 70.08, 61.82, 48.85, 47.24, 44.24, 43.14, 35.21, 32.52, 28.77, 28.22, 24.26, 22.69, 21.49, 15.52.

*(9H-Fluoren-9-yl)methyl(R,E)-1-(4-(benzyloxy)phenyl)-4-((1S,2S,5R)-2-isopropyl-5-methylcyclohexyl)-2-methylbut-3-en-2-ylcarbamate (**21**).* To a solution of the isocyanate **20** (1.36 g, 1.0 equiv, 3.16 mmol) in dry benzene (0.07 M, 48.5 mL) at room temperature under argon was added 9-fluorenemethanol (0.93 g, 1.5 equiv, 4.75 mmol) as a solid followed by dropwise addition of titanium(IV) *tert*-butoxide (0.24 mL, 0.2 equiv, 0.63 mmol). The reaction mixture was then heated at 45 °C for 3 h and quenched with a saturated NH_4Cl solution. The phases were separated, and the aqueous phase was extracted with diethyl ether (3 × 50 mL). The combined organic phases were washed with brine (75 mL), dried over $MgSO_4$, filtered, and concentrated under reduced pressure. The crude compound was purified by silica gel flash column chromatography using diethyl ether-hexanes (8:92 to 2:8 in 10 CV) to afford the desired product as a white solid. HRMS *m/z*: $[M + Na]^+$ calculated for $C_{43}H_{49}NO_3$: 627.3712, found: 627.3708; ^1H NMR ($CDCl_3$, 300 MHz, 298 K) δ (ppm) 7.77 (d, 2H, J = 7.46 Hz), 7.60 (d, 2H, J = 7.37 Hz) 7.46−7.29 (m, 9H), 6.99 (s, 2H), 6.84 (d, 2H, J = 8.51 Hz), 5.56 (d, 1H, J = 15.00 Hz), 5.21 (dd, 1H, J = 15.57, 9.57 Hz), 5.02 (s, 2H), 4.60 (s, 1H), 4.43 (s, 2H), 4.25 (t, 1H, J = 6.57 Hz), 2.98 (s, 2H), 1.89 (d, 1H, J = 9.37 Hz), 1.72 (d, 2H, J =12.49 Hz), 1.59 (m, 3H), 1.37 (s, 3H), 1.32−1.25 (m, 1H), 1.05−0.94 (m, 3H), 0.87 (d, 3H, J = 2.09Hz), 0.85 (d, 3H, J = 2.64 Hz), 0.72 (d, 3H, J = 6.85 Hz). ^{13}C NMR ($CDCl_3$, 300 MHz, 298 K) δ (ppm) 157.60, 144.19, 141.45, 137.26, 134.00, 133.70, 131.70, 129.71, 128.66, 128.01, 127.73, 127.55, 127.12, 125.13, 120.06, 114.34, 70.08, 66.04, 56.41, 47.53, 47.29, 44.68, 44.46, 43.29, 35.25, 32.54, 28.16, 25.26, 24.22, 22.72, 21.57, 15.58.

*Fmoc-D-α-MeTyr(OBn)-OH (**22**).* To a stirred solution of the carbamate **21** (1.3 g, 1.0 equiv, 2.07 mmol) and Sudan(III) (1 mg) (used as indicator) in CH_2Cl_2 (41.5 mL, 0.05 M) at −78 °C was bubbled ozone until the red-colored solution became orange (∼20 min). Triphenylphosphine (2.72 g, 5.0 equiv, 10.35 mmol) was added to the intermediate ozonide solution at 0 °C and stirred at room temperature for 15 h. The solvent was evaporated under reduced pressure, and the orange solid obtained was filtered through a small silica gel bed eluting with hexane and diethyl ether (80:20). The filtrate was concentrated under reduced pressure to afford the intermediate aldehyde (**49** in Supporting Information) (1.04 g) as a colorless oil.

[Pinnick oxidation]: To a stirred solution of the intermediate aldehyde (1.04 g, 2.07 mmol) in *t*-butanol (0.1 M, 20 mL) was added 2-methyl-2-butene (4.4 mL, 20.0 equiv, 41.4 mmol) as a neat liquid, and the mixture was cooled to 0 °C. A solution of sodium chlorite (0.75 g, 4.0 equiv, 8.28 mmol) and sodium hydrogen phosphate (1.18 g, 4.0 equiv, 8.28 mmol) in distilled water (20 mL) was added, and stirring was continued at room temperature for 15 h (the consumption of aldehyde was monitored by TLC). The mixture was concentrated under reduced pressure, and the residue was diluted with brine (50 mL) and extracted with DCM (3 × 50 mL). The combined organic phases were dried over $MgSO_4$, filtered, and concentrated under reduced pressure. The crude compound (yellow oil) was purified by silica gel flash column chromatography using methanol-DCM (2/98) to afford the title compound **22** as a white solid. HRMS *m/z*: $[M + Na]^+$ calculated for $C_{32}H_{29}NO_5$ 507.2046, found 507.2038; ^1H NMR ($CDCl_3$, 300 MHz, 298 K) δ (ppm) 7.77 (d, J = 7.50 Hz, 2H), 7.58 (t, J = 7.16 Hz, 2H) 7.46−7.34 (m, 9H), 6.95 (s, 2H), 6.83 (d, J = 8.46 Hz, 2H), 5.32 (s, 1H), 4.99 (s, 2H), 4.47 (s, 2H), 4.25 (t, J = 6.38 Hz, 1H), 3.23 (s, 2H), 1.61 (s, 3H); ^{13}C NMR ($CDCl_3$, 300 MHz, 298 K) δ (ppm) 178.13, 157.91, 143.90, 143.79, 141.39, 137.03, 131.05, 128.59, 127.97, 127.73, 127.50, 127.12, 125.00, 120.01, 114.70, 69.99, 66.53, 60.51, 47.31, 40.59, 23.52.

*Ethyl 2-Benzyl-2-nitro-3-phenylpropanoate (**56**, NO_2-Db$_z$g-OEt).* To a solution of ethyl 2-nitro-acetate (5 mL, 45.04 mmol, 1.0 equiv) in 30 mL of anhydrous DMF under argon were added DIPEA (16.1 mL, 92.33 mmol, 2.0 equiv), tetrabutylammonium iodide (TBAI, 1.7 g, 4.5 mmol, 0.1 equiv), and benzyl bromide (11 mL, 92.33 mmol, 2.0 equiv) at 0 °C. The ice-bath was removed, and the reaction mixture was stirred overnight at room temperature. Around 50 mL of HCl 0.1 M was added to quench the reaction. The product was extracted 3 times with 50 mL of Et_2O-hexane (1:1). The organic phase was washed with HCl 0.1 M, dried, and concentrated under a vacuum. The product was purified by column chromatography on silica gel. Yield: 35% (5 g). HRMS: found 336.1211 $[M + Na]^+$, calculated 336.1206. ^1H NMR ($CDCl_3$, 400 MHz, 298 K) δ (ppm): 7.35−7.28 (m, 6H), 7.22−7.15 (m, 4H), 4.13 (q, J = 7.2 Hz, 2H), 3.49 (s, 4H), 1.13 (t, J = 7.2 Hz, 3H); ^{13}C NMR ($CDCl_3$, 101 MHz, 298 K) δ (ppm): 166.48, 133.37, 130.27, 128.79, 128.01, 97.35, 62.89, 40.20, 13.70.

*Ethyl 2-Amino-2-benzyl-3-phenylpropanoate (**57**, H_2N-Db$_z$g-OEt).* To a solution of NO_2-Db$_z$g-OEt (**56**, 200 mg, 0.64 mmol, 1 equiv) in 3 mL of AcOH, Zn dust (376 mg, 5.75 mmol, 9 equiv, size <10 mm) was added for a period of 15 min. Five drops of HCl 1 M were added to accelerate the reaction. After the reaction was finished (followed up by TLC), the mixture was filtered over Celite (wetted with EtOH), and the solid was washed several times with EtOH. The combined solution was concentrated under a vacuum, resulting in precipitation of acetate salt. Saturated $NaHCO_3$ was added to liberate the free base compound, and this intermediate was extracted with EtOAc. The organic phase was washed with brine, dried with $MgSO_4$, filtered, and evaporated to dryness to afford the pure product without further purification. Yield: 70% (126 mg). HRMS: found 284.1649 $[M + H]^+$, calculated 284.1645. ^1H NMR (MeOD-d_4, 400 MHz, 298 K) δ (ppm): 7.46−7.06 (m, 10H), 4.08 (q, J = 7.2 Hz, 2H), 3.35 (d, J = 13.3 Hz, 2H), 2.83 (d, J = 13.3 Hz, 2H), 1.22 (t, J = 7.2 Hz, 3H); ^{13}C NMR (MeOD-d_4, 101 MHz, 298 K) δ (ppm): 176.39, 137.24, 131.09, 129.52, 128.22, 64.08, 62.34, 46.92, 14.46.

*Fmoc-Db$_z$g-OH (**59**).* To a solution of H_2N-Db$_z$g-OEt (**57**, 1.81 g, 6.4 mmol) dissolved in 21 mL of EtOH, 42 mL of KOH 2 M was added. The mixture was heated to reflux for 2 h. The mixture was concentrated *in vacuo* until half the volume, and 37% HCl was added dropwise at 0 °C until the product precipitates (pI ∼ 6.5). The product was filtered and rinsed with iced water. Then, 1.46 g of **58** (NH_2-Db$_z$g-OH) was obtained in a yield of 90%. The product was dried under a fume hood and was used as such in the next reaction. Free amino acid NH_2-Db$_z$g-OH (**58**, 1.46 g, 5.73 mmol, 1 equiv) was suspended in CH_2Cl_2 (10 mL), and DIPEA (3 mL, 17.18 mmol, 3 equiv) was added. Chlorotrimethylsilan (1.5 mL, 11.45 mmol, 2 equiv) was added slowly to the mixture (smoke appear) followed by 10 mL of DCM. This mixture was stirred for 10 min (until a clear solution was obtained). Fmoc-Cl (1.48 g, 5.73 mmol, 1 equiv) was added, and the mixture was stirred for 24 h and monitored by LC-MS (sample prepared in MeOH, which allows one to cleave the TMS-

https://dx.doi.org/10.1021/acs.jmedchem.0c01941
J. Med. Chem. 2021, 64, 5345−5364

protecting group). When the reaction remained unchanged, the organic phase was washed with 1 M HCl. The solvent was evaporated *in vacuo*, and the mixture was purified with MeOH-DCM (5:95) + 0.25% CH_3COOH to provide 2 g of product, yield 73%. HRMS: found 500.1842 $[M + Na]^+$, calculated 500.1832. ^1H NMR ($CDCl_3$, 400 MHz, 298 K) δ (ppm): 7.81 (d, J = 7.5 Hz, 2H), 7.57 (d, J = 7.5 Hz, 2H), 7.44 (t, J = 7.4 Hz, 2H), 7.33 (td, J = 7.5, 0.8 Hz, 2H), 7.29−7.20 (m, 6H), 7.18−7.09 (m, 4H), 5.52 (s, 1H, amide proton), 4.51 (d, J = 7.0 Hz, 2H), 4.30 (t, J = 6.9 Hz, 1H), 3.91 (d, J = 13.7 Hz, 2H), 3.27 (d, J = 13.6 Hz, 2H); ^{13}C NMR ($CDCl_3$, 101 MHz, 298 K) δ (ppm): 177.27, 154.76, 143.93, 141.47, 135.88, 129.85, 128.58, 127.89 (two peaks superposed), 127.25, 125.31, 120.13, 66.82, 66.67, 47.40, 41.24.

Synthetic Procedures and Compound Characterization (Solid-Phase Synthesis). *Materials.* 2-Chlorotrityl chloride resin (maximum loading 0.85 mmol/g, particle size 100−200 mesh), Wang resin (loading 0.3−1 mmol/g, particle size 100−200 mesh), and *O*-(7-azabenzotriazol-1-yl)-1,1,3,3-tetramethyluronium hexafluorophosphate (HATU) were obtained from Matrix Innovation (Quebec, Canada). *N*,*N*-diisopropylethylamine (DIPEA), trifluoroacetic acid (TFA), and Fmoc-protected amino acids were purchased from Chem-Impex International (Wood Dale) or Combi-Blocks (San Diego). Polypropylene cartridges 12 mL with 20 μm PE frit were purchased from Applied Separation (Allentown). Other reagents and solvents were purchased from Sigma-Aldrich (Missouri) and Fisher Scientific (Hampton). Reagents and solvents were used as received.

Solid-Phase Synthesis. The present study employs unnatural and conformationally constrained Pro12 and Phe13 mimetics to screen the binding space in the Ape13 sequence. All noncommercial amino acids were synthesized in solution and incorporated into the peptide using conventional Fmoc-based solid-phase peptide synthesis (SPPS).

All peptides were synthesized manually via Fmoc-based solid-phase peptide synthesis (SPPS) on 2-chlorotrityl chloride resin. First, the residue was loaded into the resin using 1.2 equiv of Fmoc-AA-OH and 2.5 equiv of DIPEA in DCM overnight (loading 0.45−0.70 mmol/g). Attempts to load Fmoc-Db_zg-OH on 2-chlorotrityl chloride resin were unsuccessful; thus, it was loaded to the Wang resin as described in the Supporting Information. Peptide couplings were performed with 3 equiv of Fmoc-AA-OH, 3 equiv of HATU, and 5 equiv of DIPEA for 30 min at room temperature. The reaction was monitored by the standard Kaiser test.[73] Fmoc deprotection was carried out by treatment of the resin with 4-methylpiperidine or piperidine in DMF (20:80 v/v) for 2 × 15 min. After every coupling and deprotection step, the resin was washed with DMF (3×) and CH_2Cl_2 (3×). Final cleavage (and side-chain deprotection) of the peptides from the resin was performed for 3−4 h in TFA/triethylsilane (TES)/H_2O (95:2.5:2.5 v/v) at room temperature. The resin was filtered, and the filtrate was concentrated *in vacuo*. Final peptides were purified via preparative RP-HPLC and immediately lyophilized. The peptides were obtained as white powders with a purity of >95% as determined by analytical RP-HPLC or UPLC-MS, except for **44** with purity 92%. Purity assessment was carried out on a UPLC-MS system from Waters (Milford) (column Acquity UPLC CSH C_{18} (2.1 mm × 50 mm) packed with 1.7 μm particles) with the following gradient: acetonitrile and water with 0.1% formic acid (0 → 0.2 min: 5% acetonitrile; 0.2 → 1.5 min: 5% → 95%; 1.5 → 1.8 min: 95%; 1.8 → 2.0 min: 95% → 5%; 2.0 → 2.5 min: 5%). The structures were confirmed by high-resolution electrospray mass spectrometry (maXis ESI-Q-Tof apparatus from Bruker, Billerica) and after preparing a stock solution were used as such in *in vitro* and *in vivo* assays.

***In Vitro* and *In Cellulo* Assays.** *Materials.* High-glucose Dulbecco's modified Eagle's medium (DMEM), G418, and penicillin/streptomycin were obtained from Invitrogen Life Technologies (Carlsbad). Fetal bovine serum (FBS) was purchased from Wisent (Saint-Jean-Baptiste, Canada), and bovine serum albumin (BSA) was from BioShop (Burlington, Canada). Polyethylenimine (PEI) was ordered from Polysciences (Warminster).

Cell Culture. Human embryonic kidney cells (HEK293) stably expressing yellow fluorescent protein (YFP)-tagged human APJ were cultured using the DMEM medium with 10% FBS. Cells were incubated at 37 °C under a humid atmosphere maintaining 5% CO_2. G418 (400 μg/mL) was used to create a selection pressure for cells expressing APJ, and penicillin/streptomycin (0.1%) was added to prevent bacteria contamination.

Binding Experiments. Binding experiments were carried out on HEK293 cell membranes stably expressing the YFP-tagged human APJ receptor. Cells were frozen at −80 °C for storage and only thawed right before the experiments. For membrane extraction, cells were suspended in 4 mL of EDTA solution (1 mM EDTA and 50 mM Tris-HCl, pH 7.4), transferred to a 10 mL falcon tube, and centrifuged at 3500 rpm for 15 min at 4 °C. The precipitate was suspended in binding buffer (50 mM Tris-HCl, 0.2% BSA, pH 7.4). Binding assay was carried out in 96-well plates: 15 μg of membrane proteins was incubated with 0.2 nM radiolabeled [^{125}I][Nle75, Tyr77]Pyr-apelin-13 (820 Ci/mmol)[74] and the test ligand with a range of concentrations from 10^{-5} to 10^{-11} M or 10^{-7} to 10^{-13} M in a total volume of 200 μL for 1 h at room temperature. The incubation mixtures were filtered through a glass fiber filter (Millipore, preabsorbed of PEI 0.5% for 2 h at 4 °C) to remove unbound ligands, and the filtered membranes were washed three times with 170 μL of cold binding buffer (4 °C). The γ emission was measured using a γ-counter 1470 Wizard from PerkinElmer (Waltham) (80% efficiency). Nonspecific binding did not exceed over 5% of the total signal (determined by incubation with 10^{-5} M unlabeled Pyr-apelin-13). IC_{50} values, determined from those results using GraphPad Prism 8, represent the concentration of the tested ligand displacing 50% of the radiolabeled ligand from the receptor. The K_D of Pyr-apelin-13 is 1.8 nM, determined by the saturation binding assay. The dissociation constant K_i value was calculated from IC_{50} using the Cheng−Prusoff equation, and results were displayed as mean ± SEM of two to three independent experiments, each done in duplicate.[69]

BRET Assays for $G\alpha_{i1}$ Activation and β-Arrestin2 Recruitment. HEK293 cells seeded in T175 flasks were allowed to grow in high-glucose DMEM supplemented with 10% FBS, 100 U/mL penicillin/streptomycin, 2 mM glutamine, and 20 mM 4-(2-hydroxyethyl)-1-piperazineethanesulfonic acid (HEPES) at 37 °C in a humidified chamber at 5% CO_2. All transfections were carried out with PEI. After 24 h, cells were transfected with the plasmids coding for hAPJ, $G\alpha_{i1}$-RlucII(91), GFP10-$G\gamma_2$, and $G_{\beta 1}$ (from cDNA.org) (for the BRET-based $G\alpha_{i1}$ activation assay) or coding for hAPJ-GFP10 and RlucII-β-arrestin2.[42,75,76] To perform BRET assays, cells were transferred into white 96-well plates BD Bioscience (Mississauga, Canada) at a concentration of 50 000 cells/well 24 h after transfection and incubated at 37 °C overnight. Cells were then washed with phosphate-buffered saline (PBS), and 90 μL of Hanks' balanced salt solution (HBSS) was added to each well. Then, cells were stimulated with analogues at concentrations ranging from 10^{-5} M to 10^{-11} M for 5 min at 37 °C ($G\alpha_{i1}$) or for 30 min at room temperature (β-arrestin2). After stimulation, 5 μM coelanterazine 400A was added to each well and the plate was read using the $BRET^2$ filter set of a GeniosPro plate reader (Tecan, Austria). The $BRET^2$ ratio was determined as $GFP10_{em}/RlucII_{em}$. Data were plotted, and EC_{50} values were determined using GraphPad Prism 8. Each data point represents the mean ± SEM of at least three different experiments each done in triplicate.

BRET Assay for $G\alpha_{12}$ Activation. The pcDNA3.1 plasmid encoding human APJ, human $G\alpha_{12}$, human $G_{\beta 1}$, and human $G_{\gamma 1}$ was purchased from Origene (Rockville, MD). PDZ-Rho-Gef-RLucII and rGFP-CAAX have been previously described.[77] HEK293T cells were seeded in 150 cm^2 flasks (Corning, Corning, NY), and 48 h before the experiments, they were transiently transfected with the hAPJ in combination with BRET-based biosensor cDNA in 96-well culture plates (Corning, Corning, NY) (35 000 cells/well). Transient transfections were performed using PEI at a ratio of 3:1 PEI/DNA. The total amount of transfected DNA was kept constant (100 ng/well) by the addition of salmon sperm DNA. *Measurement.* $G\alpha_{12}$ activation was assessed by monitoring ebBRET between PDZ-RhoGEF-RLucII and rGFP-CAAX coexpressed with $G\alpha_{12}$, $G\beta_1$, and $G\gamma_1$. Forty-eight hours following transfection with the appropriate biosensors and hAPJ, cells were stimulated with the ligands for 5 min.

https://dx.doi.org/10.1021/acs.jmedchem.0c01941
J. Med. Chem. 2021, 64, 5345−5364

The luciferase substrate, coelenterazine 400A (2.5 μM), was added 5 min before the reads. BRET was monitored with a Mithras LB 940 (Berthold Technologies, Bad Wildbad, Germany) equipped with a 410/70 nm donor filter and a 515/20 nm acceptor filter. The data were analyzed in GraphPad Prism 8 using "dose−response-stimulation log(agonist) vs normalized response-variable slope" with the constraint of sharing the Hill slope across all data sets. Data were presented as mean ± SEM of eight different experiments each done in simplicate.

Rat Plasma Stability. In a 96-well plate, 6 μL of compound (1 mM aqueous solution) was incubated with 27 μL of plasma (from male Sprague−Dawley rat) at 37 °C for 0, 1, 2, 4, 7, and 24 h (or 0, 5, 10, 20, 60, 120 min for less stable analogues). Degradation was quenched by adding 140 μL of acetonitrile-ethanol (1:1) solution containing *N*,*N*-dimethylbenzamide 0.25 mM (internal standard).[78] This mixture was transferred to a filter plate Impact Protein Precipitation (Phenomenex, California), and another 96-well UPLC plate was placed at the bottom to collect filtrates. Both plates were centrifuged at 500 g for 10 min at 4 °C. The filtrates were diluted with 80 μL of distilled water and analyzed using an Acquity UPLC-MS system class H (column Acquity UPLC protein BEH C4 (2.1 mm × 50 mm), 1.7 μm particles with pore 300 Å). Peptide half-life was calculated from the degradation curve using the exponential one-phase decay function in GraphPad Prism 8. Mass spectra at the time point near half-life were compared with those at 0 min (plasma-inactivated before adding the compound) to identify cleavage fragments. Data were presented as mean ± SEM of at least three different experiments each done in simplicate.

Stability against ACE2. Recombinant rat ACE2 (Sino Biological) was reconstituted in Milli-Q water and diluted to a final concentration of 20 nM in an assay buffer (100 mM Tris-HCl, 100 mM NaCl, 10 μM ZnCl2, pH 7.4). First, 1.7 μL of analogue (1 mM) was mixed with 1.7 μL of *N*,*N*-dimethylbenzamide 5 mM (internal standard) in a 96-well plate. To initiate the enzymatic reaction, 30 μL of enzyme solution was added to the mixture and incubated for 1, 2, and 24 h at 37 °C on an orbital shaker (300 rpm). At the corresponding time point, the enzyme was inactivated by adding 30 μL of EDTA 0.1 M (prepared in Milli-Q water and filtered). The blank (t = 0 min) for the ACE2 assay was prepared with similar components, but the enzyme was inactivated before adding to the mixture. The remaining peptide after incubation was quantified using a UPLC-MS system from Waters (Milford) (Acquity UPLC Protein BEH C4 column (2.1 mm × 50 mm) packed with 1.7 μm particles, pore 300 Å) with the following gradient: acetonitrile and water with 0.1% HCOOH (0 → 0.2 min: 5% acetonitrile; 0.2 → 1.5 min: 5% → 95%; 1.5 → 1.8 min: 95%; 1.8 → 2.0 min: 95% → 5%; 2.0 → 2.5 min: 5%), and the MS detector was set to the single-ion mode (SIM). Trp and Aia residues were oxidized (+16, +32) in the presence of EDTA-Zn, and a sum of oxidized and nonoxidized form was used for calculation. Experiments were repeated three times.

***In Vivo* Blood Pressure Measurement.** *Animals.* Adult male Sprague−Dawley rats, 8−10 weeks of age (Charles River Laboratories, St-Constant, Quebec, Canada), were kept on a 12 h light/12 h dark cycle with access to food and water ad libitum. The animal experimental protocols in this study were approved by the Animal Care Committee of Université de Sherbrooke and complied with policies and directives of the Canadian Council on Animal Care.

Blood Pressure Test. Male Sprague−Dawley rats (250−300 g, 8−10 weeks of age) anesthetized with ketamine/xylazine injection (87/13 mg/kg *i.m.*) were placed in supine position on a thermostatic pad. A blood pressure monitoring catheter (PE 50 filled with heparinized saline) was inserted into the right carotid artery and connected to a Micro-Med transducer (model TDX-300, Calabasas) and a Micro-Med blood pressure analyzer (model BPA-100c). Bolus injection of vehicle (isotonic saline) followed 5 min later by the injection of Ape13, compound **47**, or compound **53** (given at 19.5 nmol/kg; volume of 0.25 mL over 10 s) was carried out through another catheter (PE10) inserted into the left jugular vein. To remove residual injected substances, this *i.v.* catheter was flushed with saline (0.2 mL) immediately after each injection.

***In Vivo* Pharmacokinetics.** Male Sprague−Dawley rats weighing 250−300 g, of 8−10 weeks of age, were used in this study. A jugular vein catheter (Silastic Laboratory tubing; 0.02 in I.D. × 0.037 in O.D.) was surgically inserted 24 h prior to dosing to minimize possible anesthetic effects. This catheter was used for intravenous injections (*i.v.*, n = 3 for analogue 47 or 53 in saline solution 0.9%, ≈350 μL) and to withdraw blood. Injection volumes were determined according to the weight of the animals (3 mg/kg). Animals were placed in a containment chamber prior to *i.v.* injection to facilitate blood sampling. Blood samples (0.2 mL to obtain about 0.1 mL of plasma after centrifugation) were taken at 5, 10, 30, 60, 120, and 240 min (1, 2, 5, 10, 15 min for Pyr-apelin-13) following *i.v.* administration. Blood sample collection was made in K2-EDTA microtainer tubes (Sarstedt, Nümbrecht, Germany) and immediately placed on crushed ice before being centrifuged at 13 000 rpm for 5 min at 4 °C to isolate plasma from blood cells. The resultant plasma was then separated and transferred to polypropylene tubes and immediately frozen at −80 °C.

Sample Preparation. Plasma extraction of analogues **47** and **53** was performed by a combination of a protein precipitation and a solid-phase extraction step by LC/MS/MS analysis. The plasma sample was defrosted on ice. After vortex agitation (60 s), 100 μL was withdrawn and 300 μL of cold acetonitrile was added for protein precipitation. The sample was then vortexed (60 s) and centrifuged at 4500 rpm at 4 °C for 10 min. The supernatant was then withdrawn and directly passed through an HLB prime for additional cleanup. The filtrate was diluted 10 times in eluent A or B according to its solubility and then filtered through a 0.22 μm syringe filter before LC/MS/MS analysis.

Mass Spectrometry Analysis. Analysis of analogue **47** or **53** was performed on a Sciex Qtrap 6500+ equipped with microflow liquid chromatography (Eksigient M3 microflow). A UPLC HSS-T3 column (1 mm × 100 mm, 1.8 μm, equipped with a 0.2 μm fritted prefilter) was used for the chromatographic separation. The solvent flow rate was set to 50 μL/min, and the column temperature was kept at 40 °C. The injection volume was 3 μL. The mobile phase was 0.1% formic acid/water (A) and 0.1% formic acid/acetonitrile (B), with an elution gradient starting with 2% of eluent B, increasing to 95% in 8 min, maintaining at 95% for 2 min, and then back to initial conditions in 2 min for a total run time of 13 min. Optimized parameters were obtained by direct infusion of Ape13, **47**, and **53** analytical standard solutions at 100 ng/mL. Two daughter traces (transitions) were used (Table 1S). The most abundant transition was used for quantification and the second most abundant for confirmation.

■ ASSOCIATED CONTENT

Supporting Information

The Supporting Information is available free of charge at https://pubs.acs.org/doi/10.1021/acs.jmedchem.0c01941.

Synthetic schemes for unnatural amino acids, HRMS spectra and analytical UPLC-MS spectra, and structures of the investigated compounds (PDF)

Molecular formula strings of the investigated compounds (CSV)

■ AUTHOR INFORMATION

Corresponding Author

Philippe Sarret − *Département de Pharmacologie-Physiologie, Faculté de Médecine et des Sciences de la Santé, Université de Sherbrooke, Sherbrooke J1H 5N4, Québec, Canada; Institut de Pharmacologie de Sherbrooke, Sherbrooke J1H 5N4, Québec, Canada;* orcid.org/0000-0002-7627-701X; Email: Philippe.Sarret@USherbrooke.ca

Authors

Kien Trân − *Département de Pharmacologie-Physiologie, Faculté de Médecine et des Sciences de la Santé, Université de*

https://dx.doi.org/10.1021/acs.jmedchem.0c01941
J. Med. Chem. 2021, 64, 5345−5364

Sherbrooke, Sherbrooke J1H 5N4, Québec, Canada; Institut de Pharmacologie de Sherbrooke, Sherbrooke J1H 5N4, Québec, Canada

Robin Van Den Hauwe − *Research Group of Organic Chemistry, Departments of Chemistry and Bioengineering Sciences, Vrije Universiteit Brussel, Pleinlaan 2 1050, Brussels, Belgium*

Xavier Sainsily − *Département de Pharmacologie-Physiologie, Faculté de Médecine et des Sciences de la Santé, Université de Sherbrooke, Sherbrooke J1H 5N4, Québec, Canada; Institut de Pharmacologie de Sherbrooke, Sherbrooke J1H 5N4, Québec, Canada*

Pierre Couvineau − *Institut de Recherche en Immunologie et en Cancérologie (IRIC), Université de Montréal, Montréal H3T 1J4, Québec, Canada*

Jérôme Côté − *Département de Pharmacologie-Physiologie, Faculté de Médecine et des Sciences de la Santé, Université de Sherbrooke, Sherbrooke J1H 5N4, Québec, Canada; Institut de Pharmacologie de Sherbrooke, Sherbrooke J1H 5N4, Québec, Canada*

Louise Simard − *Institut de Pharmacologie de Sherbrooke, Sherbrooke J1H 5N4, Québec, Canada; Département de Chimie, Faculté de Science, Université de Sherbrooke, Sherbrooke J1K 2R1, Québec, Canada*

Marco Echevarria − *Institut de Pharmacologie de Sherbrooke, Sherbrooke J1H 5N4, Québec, Canada; Département de Chimie, Faculté de Science, Université de Sherbrooke, Sherbrooke J1K 2R1, Québec, Canada*

Alexandre Murza − *Département de Pharmacologie-Physiologie, Faculté de Médecine et des Sciences de la Santé, Université de Sherbrooke, Sherbrooke J1H 5N4, Québec, Canada; Institut de Pharmacologie de Sherbrooke, Sherbrooke J1H 5N4, Québec, Canada*

Alexandra Serre − *Département de Pharmacologie-Physiologie, Faculté de Médecine et des Sciences de la Santé, Université de Sherbrooke, Sherbrooke J1H 5N4, Québec, Canada; Institut de Pharmacologie de Sherbrooke, Sherbrooke J1H 5N4, Québec, Canada*

Léa Théroux − *Département de Pharmacologie-Physiologie, Faculté de Médecine et des Sciences de la Santé, Université de Sherbrooke, Sherbrooke J1H 5N4, Québec, Canada; Institut de Pharmacologie de Sherbrooke, Sherbrooke J1H 5N4, Québec, Canada*

Sabrina Saibi − *Institut de Pharmacologie de Sherbrooke, Sherbrooke J1H 5N4, Québec, Canada*

Lounès Haroune − *Institut de Pharmacologie de Sherbrooke, Sherbrooke J1H 5N4, Québec, Canada;* orcid.org/0000-0001-5420-6619

Jean-Michel Longpré − *Département de Pharmacologie-Physiologie, Faculté de Médecine et des Sciences de la Santé, Université de Sherbrooke, Sherbrooke J1H 5N4, Québec, Canada; Institut de Pharmacologie de Sherbrooke, Sherbrooke J1H 5N4, Québec, Canada*

Olivier Lesur − *Institut de Pharmacologie de Sherbrooke, Sherbrooke J1H 5N4, Québec, Canada; Département de Médecine spécialisé, Faculté de Médecine et des Sciences de la Santé, Université de Sherbrooke, Sherbrooke J1H 5N4, Québec, Canada*

Mannix Auger-Messier − *Institut de Pharmacologie de Sherbrooke, Sherbrooke J1H 5N4, Québec, Canada; Département de Médecine spécialisé, Faculté de Médecine et des Sciences de la Santé, Université de Sherbrooke, Sherbrooke J1H 5N4, Québec, Canada*

Claude Spino − *Institut de Pharmacologie de Sherbrooke, Sherbrooke J1H 5N4, Québec, Canada; Département de Chimie, Faculté de Science, Université de Sherbrooke, Sherbrooke J1K 2R1, Québec, Canada;* orcid.org/0000-0001-6249-5908

Michel Bouvier − *Institut de Recherche en Immunologie et en Cancérologie (IRIC), Université de Montréal, Montréal H3T 1J4, Québec, Canada;* orcid.org/0000-0003-1128-0100

Steven Ballet − *Research Group of Organic Chemistry, Departments of Chemistry and Bioengineering Sciences, Vrije Universiteit Brussel, Pleinlaan 2 1050, Brussels, Belgium;* orcid.org/0000-0003-4123-1641

[‡]**Éric Marsault** − *Département de Pharmacologie-Physiologie, Faculté de Médecine et des Sciences de la Santé, Université de Sherbrooke, Sherbrooke J1H 5N4, Québec, Canada; Institut de Pharmacologie de Sherbrooke, Sherbrooke J1H 5N4, Québec, Canada;* orcid.org/0000-0002-5305-8762

Complete contact information is available at: https://pubs.acs.org/10.1021/acs.jmedchem.0c01941

Author Contributions

K.T. and R.V.D. H. contributed equally to this study. E.M., P.S., and S.B. contributed equally to directing this study.

Notes

The authors declare no competing financial interest.

[‡]In memory of our close colleague, best friend and research director, Professor Éric Marsault who passed away far too early.

■ ACKNOWLEDGMENTS

Financial support from Université de Sherbrooke, the Canadian Institutes of Health Research, the Canada Foundation for Innovation, and the Fonds de la Recherche du Québec en Santé (FRQS) is gratefully acknowledged. The Canadian Francophonie Scholarship Program (PCBF), MITACS, and FRQS are also acknowledged for scholarship grants to K.T., A.M., and X.S., respectively. M.A.-M. is the recipient of a Heart and Stroke Foundation of Canada (HFSC) New Investigator award and a research scholar from the Fonds de la Recherche du Québec en Santé (FRQS). P.S. is the recipient of the Canada Research Chair in Neurophysiopharmacology of Chronic Pain. E.M. is a member of the FRQNT-funded Proteo Network and the FRQS-funded Réseau Québécois de Recherche sur le Médicament. R.V.D.H. and S.B. thank the Research Council of the Vrije Universiteit Brussel for the financial support. S.B. also acknowledges the Spearhead Research Program of VUB for continuous support.

■ ABBREVIATIONS

Ape-13, pyr-apelin-13; Ana, amino-naphthoazepinone; Aia, amino-indoloazepinone; BRET, bioluminescence resonance energy transfer; Bn, benzyl; DCM, dichloromethane; DIPEA, *N,N*-diisopropylethylamine; cAMP, cyclic adenosine monophosphate; cyp, cyclopentyl; Db_2g, α,α-dibenzylglycine; dcyp, dicyclopentyl; DMF, *N,N*-dimethylformamide; EDC, 1-ethyl-3-(3-dimethylaminopropyl)carbodiimide; ebBRET, enhanced bystander Bioluminescence Resonance Energy Transfer; E_{max}, maximum efficacy; ERK, extracellular-signal-regulated kinase; GPCR, G-protein-coupled receptor; HATU, *O*-(7-azabenzotriazol-1-yl)-1,1,3,3-tetramethyluronium hexafluorophosphate; HBSS, Hanks' balanced salt solution; HEK, human embryonic kidney; HRMS, high-resolution mass spectrometry; iPrOH,

https://dx.doi.org/10.1021/acs.jmedchem.0c01941
J. Med. Chem. 2021, 64, 5345−5364

isopropanol; PBS, phosphate-buffered saline; PEI, polyethylenimine; RlucII, Renilla luciferase; Pyr, pyroglutamic acid; SAR, structure−activity relationship; SPPS, solid-phase peptide synthesis; TBME, *tert*-butyl methyl ether; Tcc, 1,2,3,4-tetrahydro-β-carboline-3-carboxylic acid; TFA, trifluoroacetic acid; Tic, tetrahydroisoquinoline carboxylic acid; TIPS, triisopropylsilane; TES, triethylsilane; UPLC, ultrahigh-performance liquid chromatography; YFP, yellow fluorescent protein

REFERENCES

(1) Dalzell, J. R.; Rocchiccioli, J. P.; Weir, R. A. P.; Jackson, C. E.; Padmanabhan, N.; Gardner, R. S.; Petrie, M. C.; McMurray, J. J. V. The Emerging Potential of the Apelin-APJ System in Heart Failure. *J. Card. Failure* **2015**, *21*, 489−498.

(2) Taheri, S.; Murphy, K.; Cohen, M.; Sujkovic, E.; Kennedy, A.; Dhillo, W.; Dakin, C.; Sajedi, A.; Ghatei, M.; Bloom, S. The Effects of Centrally Administered Apelin-13 on Food Intake, Water Intake and Pituitary Hormone Release in Rats. *Biochem. Biophys. Res. Commun.* **2002**, *291*, 1208−1212.

(3) Lee, D. K.; Cheng, R.; Nguyen, T.; Fan, T.; Kariyawasam, A. P.; Liu, Y.; Osmond, D. H.; George, S. R.; O'Dowd, B. F. Characterization of Apelin, the Ligand for the APJ Receptor. *J. Neurochem.* **2000**, *74*, 34−41.

(4) Reaux, A.; Mota, N. D.; Skultetyova, I.; Lenkei, Z.; Messari, S. E.; Gallatz, K.; Corvol, P.; Palkovits, M.; Llorens-Cortès, C. Physiological Role of a Novel Neuropeptide, Apelin, and Its Receptor in the Rat Brain. *J. Neurochem.* **2001**, *77*, 1085−1096.

(5) Bertrand, C.; Valet, P.; Castan-Laurell, I. Apelin and Energy Metabolism. *Front. Physiol.* **2015**, *6*, 115.

(6) Szokodi, I.; Tavi, P.; Földes, G.; Voutilainen-Myllylä, S.; Ilves, M.; Tokola, H.; Pikkarainen, S.; Piuhola, J.; Rysä, J.; Tóth, M.; Ruskoaho, H. Apelin, the Novel Endogenous Ligand of the Orphan Receptor APJ, Regulates Cardiac Contractility. *Circ. Res.* **2002**, *91*, 434−440.

(7) Tatemoto, K.; Takayama, K.; Zou, M.-X.; Kumaki, I.; Zhang, W.; Kumano, K.; Fujimiya, M. The Novel Peptide Apelin Lowers Blood Pressure via a Nitric Oxide-Dependent Mechanism. *Regul. Pept.* **2001**, *99*, 87−92.

(8) Japp, A. G.; Cruden, N. L.; Amer, D. A. B.; Li, V. K. Y.; Goudie, E. B.; Johnston, N. R.; Sharma, S.; Neilson, I.; Webb, D. J.; Megson, I. L.; Flapan, A. D.; Newby, D. E. Vascular Effects of Apelin In Vivo in Man. *J. Am. Coll. Cardiol.* **2008**, *52*, 908−913.

(9) Japp, A. G.; Cruden, N. L.; Barnes, G.; van Gemeren, N.; Mathews, J.; Adamson, J.; Johnston, N. R.; Denvir, M. A.; Megson, I. L.; Flapan, A. D.; Newby, D. E. Acute Cardiovascular Effects of Apelin in Humans: Potential Role in Patients with Chronic Heart Failure. *Circulation* **2010**, *121*, 1818−1827.

(10) Folino, A.; Montarolo, P. G.; Samaja, M.; Rastaldo, R. Effects of Apelin on the Cardiovascular System. *Heart Failure Rev.* **2015**, *20*, 505−518.

(11) Marsault, E.; Llorens-Cortes, C.; Iturrioz, X.; Chun, H. J.; Lesur, O.; Oudit, G. Y.; Auger-Messier, M. The Apelinergic System: A Perspective on Challenges and Opportunities in Cardiovascular and Metabolic Disorders. *Ann. N. Y. Acad. Sci.* **2019**, *1455*, 12−33.

(12) Kawamata, Y.; Habata, Y.; Fukusumi, S.; Hosoya, M.; Fujii, R.; Hinuma, S.; Nishizawa, N.; Kitada, C.; Onda, H.; Nishimura, O.; Fujino, M. Molecular Properties of Apelin: Tissue Distribution and Receptor Binding. *BBA, Biochim. Biophys. Acta, Mol. Cell Res.* **2001**, *1538*, 162−171.

(13) Medhurst, A. D.; Jennings, C. A.; Robbins, M. J.; Davis, R. P.; Ellis, C.; Winborn, K. Y.; Lawrie, K. W. M.; Hervieu, G.; Riley, G.; Bolaky, J. E.; Herrity, N. C.; Murdock, P.; Darker, J. G. Pharmacological and Immunohistochemical Characterization of the APJ Receptor and Its Endogenous Ligand Apelin. *J. Neurochem.* **2003**, *84*, 1162−1172.

(14) Hwangbo, C.; Wu, J.; Papangeli, I.; Adachi, T.; Sharma, B.; Park, S.; Zhao, L.; Ju, H.; Go, G.; Cui, G.; Inayathullah, M.; Job, J. K.; Rajadas, J.; Kwei, S. L.; Li, M. O.; Morrison, A. R.; Quertermous, T.; Mani, A.; Red-Horse, K.; Chun, H. J. Endothelial APLNR Regulates Tissue Fatty Acid Uptake and Is Essential for Apelin's Glucose-Lowering Effects. *Sci. Transl. Med.* **2017**, *9*, No. eaad4000.

(15) Zhao, H.; Tian, X.; He, L.; Li, Y.; Pu, W.; Liu, Q.; Tang, J.; Wu, J.; Cheng, X.; Liu, Y.; Zhou, Q.; Tan, Z.; Bai, F.; Xu, F.; Smart, N.; Zhou, B. Apj+ Vessels Drive Tumor Growth and Represent a Tractable Therapeutic Target. *Cell Rep.* **2018**, *25*, 1241−1254.e5.

(16) Kleinz, M. J.; Skepper, J. N.; Davenport, A. P. Immunocytochemical Localisation of the Apelin Receptor, APJ, to Human Cardiomyocytes, Vascular Smooth Muscle and Endothelial Cells. *Regul. Pept.* **2005**, *126*, 233−240.

(17) O'Carroll, A.-M.; Selby, T. L.; Palkovits, M.; Lolait, S. J. Distribution of MRNA Encoding B78/Apj, the Rat Homologue of the Human APJ Receptor, and Its Endogenous Ligand Apelin in Brain and Peripheral Tissues. *Biochim. Biophys. Acta, Gene Struct. Expression* **2000**, *1492*, 72−80.

(18) Griffiths, P. R.; Lolait, S. J.; Bijabhai, A.; O'Carroll-Lolait, A.; Paton, J. F. R.; O'Carroll, A.-M. Increased Apelin Receptor Gene Expression in the Subfornical Organ of Spontaneously Hypertensive Rats. *PLoS One* **2020**, *15*, No. e0231844.

(19) Fischer, C. A Patent Review of Apelin Receptor (APJR) Modulators (2014-2019). *Expert Opin. Ther. Pat.* **2020**, *30*, 251−261.

(20) Maguire, J. J.; Kleinz, M. J.; Pitkin, S. L.; Davenport, A. P. [Pyr1]Apelin-13 Identified as the Predominant Apelin Isoform in the Human Heart Vasoactive Mechanisms and Inotropic Action in Disease. *Hypertension* **2009**, *54*, 598−604.

(21) Zhen, E. Y.; Higgs, R. E.; Gutierrez, J. A. Pyroglutamyl Apelin-13 Identified as the Major Apelin Isoform in Human Plasma. *Anal. Biochem.* **2013**, *442*, 1−9.

(22) Kang, Y.; Kim, J.; Anderson, J. P.; Wu, J.; Gleim, S. R.; Kundu, R. K.; McLean, D. L.; Kim, J.; Park, H.; Jin, S.; Hwa, J.; Quertermous, T.; Chun, H. J. Apelin-APJ Signaling Is a Critical Regulator of Endothelial MEF2 Activation in Cardiovascular Development. *Circ. Res.* **2013**, *113*, 22−31.

(23) Masri, B.; Lahlou, H.; Mazarguil, H.; Knibiehler, B.; Audigier, Y. Apelin (65−77) Activates Extracellular Signal-Regulated Kinases via a PTX-Sensitive G Protein. *Biochem. Biophys. Res. Commun.* **2002**, *290*, 539−545.

(24) Than, A.; Cheng, Y.; Foh, L.-C.; Leow, M. K.-S.; Lim, S. C.; Chuah, Y. J.; Kang, Y.; Chen, P. Apelin Inhibits Adipogenesis and Lipolysis through Distinct Molecular Pathways. *Mol. Cell. Endocrinol.* **2012**, *362*, 227−241.

(25) Deng, C.; Chen, H.; Yang, N.; Feng, Y.; Hsueh, A. J. W. Apela Regulates Fluid Homeostasis by Binding to the APJ Receptor to Activate Gi Signaling. *J. Biol. Chem.* **2015**, *290*, 18261−18268.

(26) Yang, Y.; Zhang, X.; Cui, H.; Zhang, C.; Zhu, C.; Li, L. Apelin-13 Protects the Brain against Ischemia/Reperfusion Injury through Activating PI3K/Akt and ERK1/2 Signaling Pathways. *Neurosci. Lett.* **2014**, *568*, 44−49.

(27) Cai, X.; Bai, B.; Zhang, R.; Wang, C.; Chen, J. Apelin Receptor Homodimer-Oligomers Revealed by Single-Molecule Imaging and Novel G Protein-Dependent Signaling. *Sci. Rep.* **2017**, *7*, No. 40335.

(28) Ji, B.; Shang, L.; Wang, C.; Wan, L.; Cheng, B.; Chen, J. Roles for Heterodimerization of APJ and B2R in Promoting Cell Proliferation via ERK1/2-ENOS Signaling Pathway. *Cell. Signalling* **2020**, *73*, No. 109671.

(29) Bai, B.; Cai, X.; Jiang, Y.; Karteris, E.; Chen, J. Heterodimerization of Apelin Receptor and Neurotensin Receptor 1 Induces Phosphorylation of ERK(1/2) and Cell Proliferation via Gαq-Mediated Mechanism. *J. Cell. Mol. Med.* **2014**, *18*, 2071−2081.

(30) Li, Y.; Chen, J.; Bai, B.; Du, H.; Liu, Y.; Liu, H. Heterodimerization of Human Apelin and Kappa Opioid Receptors: Roles in Signal Transduction. *Cell. Signalling* **2012**, *24*, 991−1001.

(31) Goupil, E.; Laporte, S. A.; Hébert, T. E. GPCR Heterodimers: Asymmetries in Ligand Binding and Signalling Output Offer New Targets for Drug Discovery: GPCR Heterodimers. *Br. J. Pharmacol.* **2013**, *168*, 1101−1103.

https://dx.doi.org/10.1021/acs.jmedchem.0c01941
J. Med. Chem. 2021, 64, 5345−5364

(32) Chen, X.; Bai, B.; Tian, Y.; Du, H.; Chen, J. Identification of Serine 348 on the Apelin Receptor as a Novel Regulatory Phosphorylation Site in Apelin-13-Induced G Protein-Independent Biased Signaling. *J. Biol. Chem.* **2014**, *289*, 31173−31187.
(33) Reiter, E.; Ahn, S.; Shukla, A. K.; Lefkowitz, R. J. Molecular Mechanism of β-Arrestin-Biased Agonism at Seven-Transmembrane Receptors. *Annu. Rev. Pharmacol. Toxicol.* **2012**, *52*, 179−197.
(34) Jia, Y. X.; Lu, Z. F.; Zhang, J.; Pan, C. S.; Yang, J. H.; Zhao, J.; Yu, F.; Duan, X. H.; Tang, C. S.; Qi, Y. F. Apelin Activates L-Arginine/Nitric Oxide Synthase/Nitric Oxide Pathway in Rat Aortas. *Peptides* **2007**, *28*, 2023−2029.
(35) Hus-Citharel, A.; Bodineau, L.; Frugière, A.; Joubert, F.; Bouby, N.; Llorens-Cortes, C. Apelin Counteracts Vasopressin-Induced Water Reabsorption via Cross Talk Between Apelin and Vasopressin Receptor Signaling Pathways in the Rat Collecting Duct. *Endocrinology* **2014**, *155*, 4483−4493.
(36) Besserer-Offroy, É.; Bérubé, P.; Côté, J.; Murza, A.; Longpré, J.-M.; Dumaine, R.; Lesur, O.; Auger-Messier, M.; Leduc, R.; Marsault, É.; Sarret, P. The Hypotensive Effect of Activated Apelin Receptor Is Correlated with β-Arrestin Recruitment. *Pharmacol. Res.* **2018**, *131*, 7−16.
(37) Ceraudo, E.; Galanth, C.; Carpentier, E.; Banegas-Font, I.; Schonegge, A.-M.; Alvear-Perez, R.; Iturrioz, X.; Bouvier, M.; Llorens-Cortes, C. Biased Signaling Favoring Gi over β-Arrestin Promoted by an Apelin Fragment Lacking the C-Terminal Phenylalanine. *J. Biol. Chem.* **2014**, *289*, 24599−24610.
(38) Lee, D. K.; Saldivia, V. R.; Nguyen, T.; Cheng, R.; George, S. R.; O'Dowd, B. F. Modification of the Terminal Residue of Apelin-13 Antagonizes Its Hypotensive Action. *Endocrinology* **2005**, *146*, 231−236.
(39) Chaves-Almagro, C.; Castan-Laurell, I.; Dray, C.; Knauf, C.; Valet, P.; Masri, B. Apelin Receptors: From Signaling to Antidiabetic Strategy. *Eur. J. Pharmacol.* **2015**, *763*, 149−159.
(40) Mughal, A.; Sun, C.; O'Rourke, S. T. Activation of Large Conductance, Calcium-Activated Potassium Channels by Nitric Oxide Mediates Apelin-Induced Relaxation of Isolated Rat Coronary Arteries. *J. Pharmacol. Exp. Ther.* **2018**, *366*, 265−273.
(41) Iturrioz, X.; Gerbier, R.; Leroux, V.; Alvear-Perez, R.; Maigret, B.; Llorens-Cortes, C. By Interacting with the C-Terminal Phe of Apelin, Phe255 and Trp259 in Helix VI of the Apelin Receptor Are Critical for Internalization. *J. Biol. Chem.* **2010**, *285*, 32627−32637.
(42) Murza, A.; Besserer-Offroy, É.; Côté, J.; Bérubé, P.; Longpré, J.-M.; Dumaine, R.; Lesur, O.; Auger-Messier, M.; Leduc, R.; Sarret, P.; Marsault, É. C-Terminal Modifications of Apelin-13 Significantly Change Ligand Binding, Receptor Signaling, and Hypotensive Action. *J. Med. Chem.* **2015**, *58*, 2431−2440.
(43) Murza, A.; Belleville, K.; Longpré, J.-M.; Sarret, P.; Marsault, É. Stability and Degradation Patterns of Chemically Modified Analogs of Apelin-13 in Plasma and Cerebrospinal Fluid. *Biopolymers* **2014**, *102*, 297−303.
(44) Wang, W.; McKinnie, S. M. K.; Farhan, M.; Paul, M.; McDonald, T.; McLean, B.; Llorens-Cortes, C.; Hazra, S.; Murray, A. G.; Vederas, J. C.; Oudit, G. Y. Angiotensin-Converting Enzyme 2 Metabolizes and Partially Inactivates Pyr-Apelin-13 and Apelin-17: Physiological Effects in the Cardiovascular System. *Hypertension* **2016**, *68*, 365−377.
(45) Xi, Y.; Yu, D.; Yang, R.; Zhao, Q.; Wang, J.; Zhang, H.; Qian, K.; Shi, Z.; Wang, W.; Brown, R.; Li, Y.; Tian, Z.; Gong, D.-W. Recombinant Fc-Elabela Fusion Protein Has Extended Plasma Half-Life Andmitigates Post-Infarct Heart Dysfunction in Rats. *Int. J. Cardiol.* **2019**, *292*, 180−187.
(46) Vickers, C.; Hales, P.; Kaushik, V.; Dick, L.; Gavin, J.; Tang, J.; Godbout, K.; Parsons, T.; Baronas, E.; Hsieh, F.; Acton, S.; Patane, M.; Nichols, A.; Tummino, P. Hydrolysis of Biological Peptides by Human Angiotensin-Converting Enzyme-Related Carboxypeptidase. *J. Biol. Chem.* **2002**, *277*, 14838−14843.
(47) Kehoe, K.; Van Elzen, R.; Verkerk, R.; Sim, Y.; Van der Veken, P.; Lambeir, A.-M.; De Meester, I. Prolyl Carboxypeptidase Purified from Human Placenta: Its Characterization and Identification as an Apelin-Cleaving Enzyme. *Biochim. Biophys. Acta, Proteins Proteomics* **2016**, *1864*, 1481−1488.
(48) McKinnie, S. M. K.; Fischer, C.; Tran, K. M. H.; Wang, W.; Mosquera, F.; Oudit, G. Y.; Vederas, J. C. The Metalloprotease Neprilysin Degrades and Inactivates Apelin Peptides. *ChemBioChem* **2016**, *17*, 1495−1498.
(49) Fischer, C.; Lamer, T.; Wang, W.; McKinnie, S. M. K.; Iturrioz, X.; Llorens-Cortes, C.; Oudit, G. Y.; Vederas, J. C. Plasma Kallikrein Cleaves and Inactivates Apelin-17: Palmitoyl- and PEG-Extended Apelin-17 Analogs as Metabolically Stable Blood Pressure-Lowering Agents. *Eur. J. Med. Chem.* **2019**, *166*, 119−124.
(50) Chapman, N. A.; Dupré, D. J.; Rainey, J. K. The Apelin Receptor: Physiology, Pathology, Cell Signalling, and Ligand Modulation of a Peptide-Activated Class A GPCR. *Biochem. Cell Biol.* **2014**, *92*, 431−440.
(51) Murza, A.; Trân, K.; Bruneau-Cossette, L.; Lesur, O.; Auger-Messier, M.; Lavigne, P.; Sarret, P.; Marsault, É. Apelins, ELABELA, and Their Derivatives: Peptidic Regulators of the Cardiovascular System and Beyond. *Pept. Sci.* **2019**, *111*, No. e24064.
(52) Charles, C. J. Update on Apelin Peptides as Putative Targets for Cardiovascular Drug Discovery. *Expert Opin. Drug Discovery* **2011**, *6*, 633−644.
(53) Scimia, M. C.; Blass, B. E.; Koch, W. J. Apelin Receptor: Its Responsiveness to Stretch Mechanisms and Its Potential for Cardiovascular Therapy. *Expert Rev. Cardiovasc. Ther.* **2014**, *12*, 733−741.
(54) Huang, Z.; He, L.; Chen, Z.; Chen, L. Targeting Drugs to APJ Receptor: From Signaling to Pathophysiological Effects. *J. Cell. Physiol.* **2019**, *234*, 61−74.
(55) Mughal, A.; O'Rourke, S. T. Vascular Effects of Apelin: Mechanisms and Therapeutic Potential. *Pharmacol. Ther.* **2018**, *190*, 139−147.
(56) Narayanan, S.; Harris, D. L.; Maitra, R.; Runyon, S. P. Regulation of the Apelinergic System and Its Potential in Cardiovascular Disease: Peptides and Small Molecules as Tools for Discovery: Miniperspective. *J. Med. Chem.* **2015**, *58*, 7913−7927.
(57) Trân, K.; Murza, A.; Sainsily, X.; Coquerel, D.; Côté, J.; Belleville, K.; Haroune, L.; Longpré, J.-M.; Dumaine, R.; Salvail, D.; Lesur, O.; Auger-Messier, M.; Sarret, P.; Marsault, É. A Systematic Exploration of Macrocyclization in Apelin-13: Impact on Binding, Signaling, Stability, and Cardiovascular Effects. *J. Med. Chem.* **2018**, *61*, 2266−2277.
(58) Murza, A.; Parent, A.; Besserer-Offroy, E.; Tremblay, H.; Karadereye, F.; Beaudet, N.; Leduc, R.; Sarret, P.; Marsault, É. Elucidation of the Structure-Activity Relationships of Apelin: Influence of Unnatural Amino Acids on Binding, Signaling, and Plasma Stability. *ChemMedChem* **2012**, *7*, 318−325.
(59) Fan, X.; Zhou, N.; Zhang, X.; Mukhtar, M.; Lu, Z.; Fang, J.; DuBois, G. C.; Pomerantz, R. J. Structural and Functional Study of the Apelin-13 Peptide, an Endogenous Ligand of the HIV-1 Coreceptor, APJ†. *Biochemistry* **2003**, *42*, 10163−10168.
(60) Kobayashi, H.; Picard, L.-P.; Schönegge, A.-M.; Bouvier, M. Bioluminescence Resonance Energy Transfer-Based Imaging of Protein-Protein Interactions in Living Cells. *Nat. Protoc.* **2019**, *14*, 1084−1107.
(61) Willemse, T.; Van Imp, K.; Goss, R. J. M.; Van Vlijmen, H. W. T.; Schepens, W.; Maes, B. U. W.; Ballet, S. Suzuki−Miyaura Diversification of Amino Acids and Dipeptides in Aqueous Media. *ChemCatChem* **2015**, *7*, 2055−2070.
(62) Lesma, G.; Sacchetti, A.; Bai, R.; Basso, G.; Bortolozzi, R.; Hamel, E.; Silvani, A.; Vaiana, N.; Viola, G. Hemiasterlin Analogues Incorporating an Aromatic, and Heterocyclic Type C-Terminus: Design, Synthesis and Biological Evaluation. *Mol. Diversity* **2014**, *18*, 357−373.
(63) Van der Poorten, O.; Knuhtsen, A.; Sejer Pedersen, D.; Ballet, S.; Tourwé, D. Side Chain Cyclized Aromatic Amino Acids: Great Tools as Local Constraints in Peptide and Peptidomimetic Design. *J. Med. Chem.* **2016**, *59*, 10865−10890.

https://dx.doi.org/10.1021/acs.jmedchem.0c01941
J. Med. Chem. 2021, 64, 5345−5364

(64) Van der Poorten, O.; Legrand, B.; Vezenkov, L. L.; García-Pindado, J.; Bettache, N.; Knuhtsen, A.; Pedersen, D. S.; Sánchez-Navarro, M.; Martinez, J.; Teixidó, M.; Garcia, M.; Tourwé, D.; Amblard, M.; Ballet, S. Indoloazepinone-Constrained Oligomers as Cell-Penetrating and Blood−Brain-Barrier-Permeating Compounds. *ChemBioChem* **2018**, *19*, 696−705.
(65) Van der Poorten, O.; Van Den Hauwe, R.; Eiselt, E.; Betti, C.; Guillemyn, K.; Chung, N. N.; Hallé, F.; Bihel, F.; Schiller, P. W.; Tourwé, D.; Sarret, P.; Gendron, L.; Ballet, S. χ-Space Screening of Dermorphin-Based Tetrapeptides through Use of Constrained Arylazepinone and Quinolinone Scaffolds. *ACS Med. Chem. Lett.* **2017**, *8*, 1177−1182.
(66) Postnova, M. V.; Koshel', S. G.; Lebedeva, N. V.; Kuznetsova, E. A.; Koshel', G. N. Synthesis of Cyclohexylphenols. *Russ. J. Org. Chem.* **2003**, *39*, 1415−1417.
(67) Spino, C. Menthone and p-Menthyl-3-Carboxaldehyde as Chiral Auxiliaries. *Chem. Commun.* **2011**, *47*, 4872−4883.
(68) Ban, T.; Li, X.; Ma, X.; Yang, H.; Song, Y.; Sun, Y.; Shen, M.; Li, N.; Zhang, M.-Y.; Ma, Y.; Zhong, W.; Zhang, M.; Hu, L. A. GPCR Structure and Function Relationship: Identification of a Biased Apelin Receptor Mutant. *Biochem. J.* **2018**, *475*, 3813−3826.
(69) Yung-Chi, C.; Prusoff, W. H. Relationship between the Inhibition Constant (KI) and the Concentration of Inhibitor Which Causes 50 per Cent Inhibition (I50) of an Enzymatic Reaction. *Biochem. Pharmacol.* **1973**, *22*, 3099−3108.
(70) Ma, Y.; Yue, Y.; Ma, Y.; Zhang, Q.; Zhou, Q.; Song, Y.; Shen, Y.; Li, X.; Ma, X.; Li, C.; Hanson, M. A.; Han, G. W.; Sickmier, E. A.; Swaminath, G.; Zhao, S.; Stevens, R. C.; Hu, L. A.; Zhong, W.; Zhang, M.; Xu, F. Structural Basis for Apelin Control of the Human Apelin Receptor. *Structure* **2017**, *25*, 858−866.e4.
(71) Murza, A.; Sainsily, X.; Coquerel, D.; Côté, J.; Marx, P.; Besserer-Offroy, É.; Longpré, J.-M.; Lainé, J.; Reversade, B.; Salvail, D.; Leduc, R.; Dumaine, R.; Lesur, O.; Auger-Messier, M.; Sarret, P.; Marsault, É. Discovery and Structure−Activity Relationship of a Bioactive Fragment of ELABELA That Modulates Vascular and Cardiac Functions. *J. Med. Chem.* **2016**, *59*, 2962−2972.
(72) Charles, C. J.; Rademaker, M. T.; Richards, A. M. Apelin-13 Induces a Biphasic Haemodynamic Response and Hormonal Activation in Normal Conscious Sheep. *J. Endocrinol.* **2006**, *189*, 701−710.
(73) Kaiser, E.; Colescott, R. L.; Bossinger, C. D.; Cook, P. I. Color Test for Detection of Free Terminal Amino Groups in the Solid-Phase Synthesis of Peptides. *Anal. Biochem.* **1970**, *34*, 595−598.
(74) Read, C.; Nyimanu, D.; Williams, T. L.; Huggins, D. J.; Sulentic, P.; Macrae, R. G. C.; Yang, P.; Glen, R. C.; Maguire, J. J.; Davenport, A. P. International Union of Basic and Clinical Pharmacology. CVII. Structure and Pharmacology of the Apelin Receptor with a Recommendation That Elabela/Toddler Is a Second Endogenous Peptide Ligand. *Pharmacol. Rev.* **2019**, *71*, 467−502.
(75) Zimmerman, B.; Beautrait, A.; Aguila, B.; Charles, R.; Escher, E.; Claing, A.; Bouvier, M.; Laporte, S. A. Differential β-Arrestin−Dependent Conformational Signaling and Cellular Responses Revealed by Angiotensin Analogs. *Sci. Signaling* **2012**, *5*, ra33.
(76) Galés, C.; Van Durm, J. J. J.; Schaak, S.; Pontier, S.; Percherancier, Y.; Audet, M.; Paris, H.; Bouvier, M. Probing the Activation-Promoted Structural Rearrangements in Preassembled Receptor−G Protein Complexes. *Nat. Struct. Mol. Biol.* **2006**, *13*, 778−786.
(77) Namkung, Y.; Le Gouill, C.; Lukashova, V.; Kobayashi, H.; Hogue, M.; Khoury, E.; Song, M.; Bouvier, M.; Laporte, S. A. Monitoring G Protein-Coupled Receptor and β-Arrestin Trafficking in Live Cells Using Enhanced Bystander BRET. *Nat. Commun.* **2016**, *7*, No. 12178.
(78) Juhl, C.; Els-Heindl, S.; Schönauer, R.; Redlich, G.; Haaf, E.; Wunder, F.; Riedl, B.; Burkhardt, N.; Beck-Sickinger, A. G.; Bierer, D. Development of Potent and Metabolically Stable APJ Ligands with High Therapeutic Potential. *ChemMedChem* **2016**, *11*, 2378−2384.

https://dx.doi.org/10.1021/acs.jmedchem.0c01941
J. Med. Chem. 2021, 64, 5345−5364